A model for uranium, rhenium, and molybdenum diagenesis in marine sediments based on results from coastal locations

Jennifer L. Morford[a*]
William R. Martin[b]
Roger François[b†]
Caitlin M. Carney[a]

[a]Franklin & Marshall College, Department of Chemistry, P.O. Box 3003,
Lancaster, PA USA 17604-3003
[b]Woods Hole Oceanographic Institution
Marine Chemistry and Geochemistry Department, Woods Hole, MA USA 02543

[†]Currently at Department of Earth and Ocean Sciences, University of British Columbia,
Vancouver, British Columbia, Canada V6T 1Z4

[*]Corresponding author: jennifer.morford@fandm.edu
phone: (717) 358-4590; fax: (717) 291-4343

Submitted to Geochimica et Cosmochimica Acta February 8, 2008
Resubmitted to Geochimica et Cosmochimica Acta, December 31, 2008

ABSTRACT

The purpose of this research is to characterize the mobilization and immobilization processes that control the authigenic accumulation of uranium (U), rhenium (Re) and molybdenum (Mo) in marine sediments. We analyzed these redox–sensitive metals (RSM) in benthic chamber, pore water and solid phase samples at a site in Buzzards Bay, Massachusetts, U.S.A., which has high bottom water oxygen concentrations (230–300 μmol/L) and high organic matter oxidation rates (390 μmol C/cm^2/y). The oxygen penetration depth varies from 2–9 mm below the sediment–water interface, but pore water sulfide is below detection (< 2 μM). The RSM pore water profiles are modeled with a steady–state diagenetic model that includes irrigation, which extends 10–20 cm below the sediment–water interface. To present a consistent description of trace metal diagenesis in marine sediments, RSM results from sediments in Buzzards Bay are compared with previous research from sulfidic sediments (Morford et al., *GCA* **71**).

Release of RSM to pore waters during the remineralization of solid phases occurs near the sediment–water interface at depths above the zone of authigenic RSM formation. This release occurs consistently for Mo at both sites, but only in the winter for Re in Buzzards Bay and intermittently for U. At the Buzzards Bay site, Re removal to the solid phase extends to the bottom of the profile, while the zone of removal is restricted to ~2–9 cm for U and Mo. Authigenic Re formation is independent of the anoxic remineralization rate, which is consistent with an abiotic removal mechanism. The rate of authigenic U formation and its modeled removal rate constant increase with increasing anoxic remineralization rates, and is consistent with U reduction being microbially mediated. Authigenic Mo formation is related to the formation of sulfidic microenvironments. The depth and extent of Mo removal from pore water is closely associated with the balance between iron and sulfate reduction and the consumption of pore water sulfide via iron sulfide formation. Pore water RSM reach constant asymptotic concentrations in sulfidic sediments, but only pore water Re is constant at depth in Buzzards Bay. The increases in pore water U at the Buzzards Bay site are consistent with addition via irrigation and subsequent upward diffusion to the removal zone. Deep pore

water Mo concentrations exceed its bottom water concentration due to irrigation–induced oxidation and remobilization from the solid phase. In sulfidic sediments, there is no evidence for higher pore water U or Mo concentrations at depth due to the absence of irrigation and/or the presence of more stable authigenic RSM phases.

There are good correlations between benthic fluxes and authigenic accumulation rates for U and Mo in sulfidic sediments. However, results from Buzzards Bay suggest irrigation ultimately results in the partial loss of U and Mo from the solid phase, with accumulation rates that are 20–30% of the modeled flux. Irrigation can augment (Re, possibly U) or compromise (U, Mo) authigenic accumulation in sediments, and is important when determining burial rates in continental margin sediments.

1. INTRODUCTION

Concentrations of redox–sensitive trace metals (RSM) in sediment cores have been used to determine the magnitude of and drivers for past changes in reducing conditions. Uranium (U), rhenium (Re) and molybdenum (Mo) have received attention as promising paleotracers (e.g., Calvert and Pedersen, 1993; François et al., 1997; Dean et al., 1997, 1999; Rosenthal et al., 1995; Crusius et al., 1996; Anderson et al., 1998; Crusius and Thomson, 2000; Adelson et al., 2001; Nameroff et al., 2004; Meyers et al., 2005; Algeo and Lyons, 2006; Tribovillard et al., 2006). These RSM are all generally conservative species in the ocean. Most simply, U, Re and Mo are soluble under oxic conditions and precipitate (or adsorb) under anoxic conditions (bottom water oxygen concentration equals zero, $O_{2,bw} = 0$). Inconsistent and contradictory conclusions from RSM distributions in sediments are presumably due to a lack of known mechanisms for RSM accumulation in and/or remobilization from sediments (François et al., 1997 vs. Chase et al., 2001; Nameroff et al., 2002). Understanding RSM geochemical cycling is further complicated by our present understanding of their respective ocean mass balances. Previous global mass balances based on sediments from greater than 1000 m water depth have suggested that sinks balance sources for U and Mo, whereas sinks are greater than sources for Re (Morford and Emerson, 1999). The role of sediments from less than 1000 m water depth as sinks, sources or neutral zones for RSM has not been as thoroughly investigated. The role of continental margin sediments has been recently re–evaluated to emphasize that these sediments represent a sink larger than anoxic sediments for Mo, but its magnitude is still uncertain (see discussion in McManus et al., 2006).

Diagenetic reactions that obscure the connection between authigenic metal accumulation and reducing conditions at the time of accumulation may further complicate the interpretation of RSM in sediments. Diagenetic alteration is of particular importance in coastal areas with seasonal variations in organic carbon flux to sediments, bottom water oxygen concentration, oxygen penetration depth and extent of bioturbation and irrigation. For example, under oxic conditions surface sediment layers of manganese oxides and/or iron oxyhydroxides (which will be referred to more generally as oxides throughout this paper) provide reactive surfaces for trace metal adsorption. Seasonal shoaling in the oxygen penetration depth ($O_{2,pen}$) results in reductive dissolution of Mn

and/or Fe oxides, thereby releasing adsorbed species to pore waters and overlying waters. Insight on the potential for RSM remobilization from sediments would clarify processes that can compromise RSM accumulation in sediments.

In this paper, we present solid phase and pore water results from sediments from Buzzards Bay, Massachusetts (U.S.A.) from late winter (March 2003), early spring (April 2001) and summer (August 2003, 2004). The pore water results are interpreted by applying a one–dimensional diffusion–reaction model that includes irrigation to discern controls on RSM cycling in marine sediments. The results from Buzzards Bay are compared with results from another coastal setting with sulfidic sediments (Hingham Bay, Massachusetts; Morford et al., 2007). Differences in RSM behavior between Buzzards and Hingham bays can be explained by differences in both irrigation and redox conditions. Possible explanations are tested through a systematic examination of the seasonal variability of rates of benthic processes and the effects of irrigation based on results from traditionally sliced and centrifuged sediment cores, polyacrylamide gel probes, and benthic chambers. With these results, we present a consistent description of RSM diagenesis in marine sediments.

1.1. Background

Previous information on the geochemical behavior of RSM has been dominated by two approaches: 1) field–based research and 2) experiment–based research. Field–based research, which couples extensive analyses of RSM with information on ancillary species in well–studied areas, has yielded insight regarding the cycling of RSM in sediments. U can be delivered to sediments via solute diffusion from bottom water and as a particulate non–lithogenic phase (Klinkhammer and Palmer, 1991) that is labile under oxic conditions but is preserved in sedimentary solids when bottom water O_2 concentrations are < 25 mM (Anderson, 1982; Zheng et al., 2002b). U is removed from pore waters coincident with either Fe reduction or sulfate reduction (e.g., Cochran et al., 1986; Klinkhammer and Palmer, 1991; Barnes and Cochran, 1993; Zheng et al., 2002a). Previously accumulated solid phase U can be released to bottom waters or pore waters through the oxidation of reduced U solid phases (Shaw et al., 1994). This remobilization may be observed through increasing pore water U concentrations below its depth of

136 removal (Cochran et al., 1986; Barnes and Cochran, 1991; Zheng et al., 2002a; Chaillou
137 et al., 2002). Re accumulation in sediments occurs below the U removal depth, whereas
138 either low oxygen or sulfidic bottom waters are required for Mo accumulation in
139 sediments (Emerson and Huested, 1991; Crusius et al., 1996; Zheng et al., 2000; Morford
140 et al., 2005). In turbidites, the reimmobilization process after oxidation occurs over a
141 relatively short depth range for U whereas the reimmobilization of Re occurs over a
142 longer depth range (Crusius and Thomson, 2000), which is consistent with slower
143 precipitation kinetics for Re (Sundby et al., 2004).
144 Detailed laboratory experiments have resulted in proposed mechanisms that
145 control RSM geochemical cycling. U reduction is microbially mediated, as Fe(III)– and
146 sulfate–reducing bacteria obtain energy from the reduction of U(VI) to U(IV) or (III)
147 (e.g., Lovely et al., 1991; Francis et al., 1994; Tucker et al., 1996; Senko et al., 2002;
148 Sani et al., 2004). The oxidation of previously reduced U is rapid and results in a release
149 of U to the aqueous phase (Cochran et al., 1986; Anderson et al., 1989). Experimentation
150 suggests that Re removal to the solid phase is slow under reducing conditions (Yamashita
151 et al., 2007). Wharton et al. (2000) observed that Re loss from the solid phase is limited
152 during oxidation of Re–S–Fe clusters. Mo can transition from a conservative molybdate
153 anion to a particle–reactive thiomolybdate anion (MoO_4^{2-} to $MoO_{4-x}S_x^{2-}$, x=1–4; Helz et
154 al., 1996) in the presence of H_2S. Iron sulfide mineral phases can adsorb molybdate, but
155 thimolybdates are more effectively scavenged from the aqueous phase (Helz et al., 2004).
156 Bostick et al. (2003) further showed that molybdate adsorbs weakly and reversibly to
157 FeS_2, whereas tetrathiomolybdate is irreversibly retained on FeS_2 through the formation
158 of surface Mo–Fe–S cubane structures.
159 A few studies have successfully combined both the field– and experimental–based
160 approaches to generate mechanistic interpretations of RSM distributions in sediments and
161 pore waters (Cochran et al., 1986; Barnes and Cochran, 1993; Helz et al., 1996;
162 Yamashita et al., 2007). The research presented here also represents a bridge between
163 these two research approaches. Our field–based approach focuses on RSM and
164 associated species in a seasonal study of sediments from Buzzards Bay. Our pore water
165 profiles are further interpreted using a one–dimensional diffusion–reaction model that

includes irrigation. These results suggest a coherent model regarding the diagenesis of RSM.

1.2. Study Site

Buzzards Bay is located in southern Massachusetts, USA, in the northwest Atlantic Ocean (41°31′10.3″N, 70°45′52.0″W; Figure 1; Table 1). It experiences a productivity maximum that extends from June to November or December (Roman and Tenore, 1978). The carbon flux to the sediment–water interface at this site has been measured as 400–600 μmol C/cm^2/yr (McNichol et al., 1988), and the carbon flux was 390 μmol C/cm^2/yr during this work. The water depth at the sampling site is 15 m and is near Weepecket Island. Nearby locations have been sites for numerous studies of sediment geochemistry (McNichol et al., 1988; Rowe and McNichol, 1991) and seasonal changes in bioturbation and irrigation (Martin and Sayles, 1987; Martin and Banta, 1992). Bottom water temperatures vary in a sinusoidal manner, with a minimum of 4°C in January and a maximum of ~22°C in July (this study; Banta, 1991; Rosenfeld et al., 1984). Bottom water salinity varies slightly during the year and has a mean value of 31.6 ± 0.3 psu (Rosenfeld et al., 1984). Results from this work show maximum bottom water oxygen concentrations were measured in March (302 μmol/L) relative to minimum concentrations in August (230 μmol/L).

The sediments are 17% silt and 93% silt/clay (Moore, 1963). The sedimentation rate in this area of Buzzards Bay is between 0.05 cm/yr as determined by ^{14}C (McNichol et al., 1988) and 0.3 cm/yr as determined by ^{210}Pb (Brownawell, 1986). Deposit–feeders dominate in sediments, accounting for 70–90% of the benthic fauna (Sanders, 1958).

2. METHODS AND ANALYTICAL PROCEDURES

2.1. Sampling Methods

Visually undisturbed cores were collected by SCUBA divers with 10.7 cm–diameter polycarbonate core liners. Cores were kept cool by surrounding them with ice packs during transport to a refrigerated room (~4°C) where they were sampled in a N_2

198 atmosphere within 4 hours of collection exactly as described in Morford et al. (2007).
199 Sampling resolution was 0.3 cm over the top ~1.5 cm, 0.5 cm from ~1.5 to 4 cm, and 1–2
200 cm deeper than 4 cm. Pore waters were sampled under N_2 for nitrate+nitrite, ammonium,
201 sulfate, sulfide, TCO_2 and trace metals (Morford et al., 2007). An additional core was
202 allowed to come to room temperature ~24 hours after collection to determine porosity
203 and sediment resistivity.
204 Two additional sediment cores were incubated in the cold room for ~24 hours,
205 during which time the water overlying the sediments was continuously exchanged with a
206 large reservoir of recovered bottom water from Buzzards Bay. In April 2001, oxygen
207 was also bubbled into the overlying waters during the incubation. Of the two incubated
208 cores, the pore waters in one core were equilibrated with polyacrylamide gel housed in a
209 pair of acrylonitrile butadiene styrene probes (DGT Research, Ltd., modified as described
210 in Morford et al., 2003). Following a 24–hour equilibration period (Morford et al., 2003),
211 the probes were removed from the sediments and discrete gel sections were stored in pre–
212 weighed microcentrifuge vials that contained dilute HNO_3 (5% Fisher Optima grade) for
213 trace metal analysis. The sampling resolution varied from 0.3 cm at the top to 1 cm at the
214 bottom (Morford et al., 2003). The second incubated core was sectioned and sampled at
215 the end of the 24–hour period to determine any change in the reducing conditions in the
216 sediments due to the incubation (Morford et al., 2003).
217 Benthic fluxes were measured directly using *in situ* benthic flux chambers (Sayles
218 and Dickinson, 1991), operating in O_2–controlled mode. The concentration of O_2 in the
219 chamber water was held steady by continuous pumping of bottom water through silicone
220 tubing, coiled within the overlying water in the chamber. A steady–state was reached, in
221 which the rate of addition of O_2 by diffusion across the tubing equaled the rate of loss by
222 sedimentary O_2 consumption (Morford et al., 2007). NaBr was added to the overlying
223 water at the start of each deployment to increase the dissolved Br^- concentration to ~5
224 times its *in situ* concentration. Transport of solutes across the sediment-water interface
225 and within the sediments by nondiffusive processes was quantified by studying the
226 temporal and spatial distributions of the Br^- concentrations. Experimental procedures

and interpretations of these results are described in Martin and Banta, 1992; Sayles and Martin, 1995; Martin and Sayles, 2004; Morford et al., 2007.

An *in situ* microelectrode profiling instrument was used to determine pore water oxygen and oxygen penetration depth ($O_{2,pen}$). Each deployment resulted in duplicate or triplicate profiles of pore water oxygen.

2.2. Analytical Procedures

Pore water nutrients were determined with an uncertainty of ≤ 3% for duplicate samples by autoanalyzer using methods adapted from Glibert and Loder (1977). TCO_2 was analyzed using a Licor analyzer (O'Sullivan and Millero, 1998; Morford et al., 2007). The range was ±10 µmol/kg for flux chamber samples and was ±20 µmol/kg for duplicate pore water samples. Oxygen analyses were by small–volume Winkler titration on duplicate samples with a range of ±2%. Dissolved sulfide was measured using the Cline (1969) method with a detection limit of 2 µM. Br^- was determined by ion chromatography on duplicate samples with an uncertainty of ±3%.

All pore water samples and U, Mo and Re in solid phase digests were analyzed using either a Finnigan ELEMENT I (April 2001 samples) or an ELEMENT II (all others) high–resolution inductively coupled plasma–mass spectrometer (ICP–MS) at the Woods Hole Oceanographic Institution. A separate aliquot of the solid phase digest was analyzed for Al, Fe and Mn using a Spectro Ciros CCD ICP–optical emission spectrometer (ICP–OES) at Franklin & Marshall College. Replicate measurements of CASS–4 (Nearshore Seawater Reference Material for Trace Metals, National Research Council Canada, NRCC) and overlying water samples were used to determine accuracy and precision for the pore water and benthic chamber measurements. Replicate measurements of PACS–2 (Marine Sediment Reference Materials for Trace Metals and other Constituents, NRCC) were used to assess accuracy and precision of the solid phase digest samples.

2.2.1. Trace metal analyses in pore water and benthic chamber samples

U and Mo benthic chamber samples and pore water samples from August 2004 were measured using isotope dilution (^{236}U and ^{95}Mo, respectively), and duplicate

analyses of samples suggested the precision was ≤ 3% (4 sets of duplicates). Pore water and gel probe samples were 20–fold diluted with 5% HNO_3 (Fisher Optima grade) and analyzed using a modified version of the Rodushkin and Ruth (1997) method. Internal standards (Sc, In, Cs, Lu) were used to quantify Mn, Fe, U, Mo and Re (most of the Re samples were preconcentrated prior to analysis, see later section). Measurements of overlying water samples and benthic chamber samples that were taken one hour after deployment approximate expected seawater concentrations (Table 2). Replicate measurements of the standard seawater solution CASS–4 indicate that the instrumental method precision for a 20–fold diluted seawater solution was < 6% for Mo, < 9% for U and < 17% for Mn. The measured U concentration was similar to the suggested value for the CASS–4 standard. The average concentrations of Mo and Mn were within their respective certified 95% confidence ranges. The measured Mn concentration (0.048 ± 0.008 μmol/kg) had worse precision than the certified 95% confidence range (0.0496 ± 0.003 μmol/kg) due to the extremely low concentration in the standard. Many of the samples analyzed during this research had at least an order of magnitude higher concentration. Replicate pore water samples (13 sets of duplicates) suggested similar precision relative to replicate CASS–4 measurements: < 11% for Mn and Fe when concentrations were greater than 5 μmol/kg, < 7% for Mo, and < 9% for U except for two pairs of replicates that were < 15% for U.

2.2.2. Solid phase analyses

The solid sample remaining after centrifugation was freeze–dried and ground for solid phase analyses. Dried solid phase samples were completely dissolved using a modification of the method of Murray and Leinen (1993) as described by Morford and Emerson (1999), which included concentrated HF, HCl, HNO_3 and 30% H_2O_2. The peroxide was A.C.S. grade. All of the acids used during the dissolution were trace–metal grade, but the final dilution was completed with Fisher Optima grade nitric acid. The average measured concentrations of the PACS–2 standard were within the 95% confidence level for the standard for Mo, Al, Fe and Mn (Table 3). The U concentration was lower than the recommended value for PACS–2. The precision for replicate analyses

of PACS–2 was < 2% for Al, Fe, Mn, and Re, and < 5% for U and Mo. The reproducibility of duplicate samples (5 sets) was ≤ 7% for all metals.

Excess ^{234}Th and ^{210}Pb were analyzed by direct counting on Canberra LeGe detectors (Sayles et al., 2001). Porosity and resistivity were determined by the methods of Manheim et al. (1974) and Andrews and Bennett (1981), respectively, using procedures described previously (Martin and Sayles, 2004).

2.2.3. Rhenium analyses

April 2001 pore water samples were analyzed for Re using the modified Rodushkin and Ruth (1997) method. Other pore water, benthic chamber, and all dissolved solid phase samples were manually preconcentrated for Re (Morford et al. 2005; Colodner et al. 1993). Samples were combined with an isotope spike enriched in ^{185}Re and preconcentrated using AG1-X8 100–200 mesh chloride–form resin (Biorad). The resin had been cleaned and conditioned with HNO_3 (Fisher Optima grade).

Samples of CASS–4 were analyzed repeatedly to determine the precision of the Re preconcentration method. Although this standard is not certified for Re, the average measured concentration was similar to the expected Re concentration adjusting for the salinity of the CASS–4 standard (Table 2). Duplicate sample measurements suggested that the range of the preconcentration method was always within 2%. The average concentrations of overlying water and benthic chamber (t=1 hour) samples are similar to the expected Re concentration, adjusting for the average salinity in Buzzards Bay (Table 2). Samples of PACS–2 were analyzed repeatedly to determine the precision of the solid phase digestion and preconcentration method, which was < 2%. The range for duplicate analyses of five different samples that were individually dissolved and preconcentrated was ≤ 7%.

2.2.4. Determining U oxidation states in pore waters

Uranium speciation was determined for pore water samples recovered in August 2004 following the method of Cochran et al. (1986). Whereas the Cochran et al. (1986) method required 100–200 mL of pore water, this method was applied to two–mL samples of filtered pore water that were adjusted to 4 M HCl by adding trace metal grade 12 M

HCl. All column separations were done in a N_2–filled glove bag. Each sample was loaded onto a column (Dowex 1x8–200 ion exchange resin, Acros Organics) and washed with 4 M HCl to remove U(IV) but retain U(VI) on the resin. Aliquots of 0.1 M HCl were used to elute the U(VI) fraction. A second series of three aliquots of 0.1 M HCl was added to the column to verify that all of the U(VI) was eluted. A check sample suggested that 99% of the U(VI) was removed in the first elution. A ^{236}U isotope spike was gravimetrically added to the U(VI)–containing effluent and no further sample purification was done prior to analysis using the ICP–MS at WHOI. The U(VI) concentration was determined and compared to the total U concentration measured in a separate fraction of the sample prior to column separation. The U(IV) fraction was not separately quantified.

3. A MODEL FOR U, MO AND RE DIAGENESIS

The pore water profiles for U, Mo and Re are interpreted using a one–dimensional steady–state model. This modeling effort is a means to (1) use a curve–fitting procedure to estimate the profile slopes at the sediment–water interface and at the top of the removal layer, and (2) provide a quantitative means of comparing the behaviors of the three RSM. In applying a steady–state model to the temporally variable Buzzards Bay sediments, we assume that the time scale of seasonal change is long relative to the RSM reaction rates. This model is similar to the model presented in Morford et al. (2007), with the exception that nondiffusive transport has been incorporated into the model to improve the interpretation of the Buzzards Bay pore water profiles.

The steady–state diagenetic pore water model takes the form:

$$(1) \qquad 0 = \frac{d}{dx}\left\{\phi D_{i,sed}\frac{dC_i}{dx}\right\} - \frac{d}{dx}\{\phi \upsilon C_i\} + \phi R_i + \phi \alpha_i (C_{bw} - C_i)$$

At the surface (x=0), the pore water concentration equals the bottom water concentration ($C=C_{bw}$). At the bottom boundary ($x = x_{max}$), $dC/dx = 0$. The sediment porosity is ϕ (cm^3_{pw}/cm^3_{sed}), and $D_{i,sed}$ is the sedimentary diffusion coefficient of solute i. The concentration of the solute in pore waters is C_i, and its concentration in bottom water is C_{bw}. Concentration units are nmol or $pmol/cm^3_{soln}$. R_i is the reaction rate of solute i (nmol or $pmol/cm^3_{soln}/y$). The irrigation rate parameter for solute i is α_i (1/y). The pore water

354 burial rate (υ) is calculated from the sediment burial rate (Berner, 1980) determined from
355 radiocarbon data by McNichol et al. (1988).

356 *Diffusion coefficients:* The sedimentary diffusion coefficient ($D_{i,sed}$) is calculated
357 from the pore water diffusion coefficient ($D_{i,pw}$) as follows:

358 (2) $$D_{i,sed} = \frac{D_{i,pw}}{\phi F} = D_{i,pw}\phi^{\nu-1}$$

359

360 The pore water diffusion coefficient (D_{pw}) is assumed to be equal to the ionic
361 diffusion coefficient in seawater (D_{sw}). The seawater diffusion coefficient for Mo (9.91 x
362 10^{-6} cm^2/s at 25°C) was taken from Li and Gregory (1974). The D_{sw} for U was assumed
363 to be equivalent to that of Mo (Morford et al., 2007). The diffusion coefficient for Re
364 was calculated based on the limiting equivalent conductance of ReO_4^- (Nigrini, 1970;
365 $D(ReO_4^-) = 14.6 \times 10^{-6}$ cm^2/s at 25°C). The diffusion coefficients were then calculated
366 for *in situ* temperatures following Li and Gregory (1974). During each sampling time at
367 the Buzzards Bay site, both the sediment porosity (ϕ) and the formation factor (F) were
measured to quantify the effect of sediment tortuosity on D_{sed} (Figure 2, Table 4).

368 *Transport by sediment irrigation*: The rate of this process is equal to the product
369 of an irrigation parameter (α, 1/y) and the pore water–bottom water concentration
370 difference (Christensen et al., 1984; Emerson et al., 1984; Boudreau, 1984). The
371 irrigation rate parameter, α_i, was determined for this site as follows:

372 (3) $$\alpha_i = \alpha_{Br}\frac{D_{i,sw}}{D_{Br,sw}}$$

373 The irrigation rate parameter for Br^- was determined using Br^- tracer experiments
374 (this study) and calculated from $^{222}Rn/^{226}Ra$ disequilibrium measurements (Martin and
375 Sayles, 1987; see later discussion).

376 *Reaction rates:* The depth-dependence of the reaction rate is the same as that
377 adopted by Morford et al. (2007). There are three sedimentary layers in which distinct
378 reactions occur. Near the sediment–water interface, RSM may be mobilized from solids
379 to the solution phase. This reaction is assumed to be zero–order in dissolved RSM
380 concentration (equation 4). In a deeper layer, RSM may be removed from pore waters to
381 authigenic phases. The removal zone extends from x_p to x_s and is modeled as first–order

in the difference between the pore water RSM concentration (C_i) and a quasi–equilibrium concentration that is assumed to be the minimum measured concentration in the profile (C_{min}; equation 5). We assume no that there is no reaction in the deepest layer (equation 6). This assumption is discussed in detail below.

$$0 \le x \le x_p,\ R_i = k_r \quad (4)$$

$$x_p \le x \le x_s,\ R_i = k_p\left(C_i - C_{\min}\right) \quad (5)$$

$$x_s < x,\ R_i = 0 \quad (6)$$

All pore water profiles for each RSM at each time point were combined into a "composite" profile. Then, least-squares fits to the profile were used to obtain optimal values for the four parameters, x_s, x_p, k_r and k_p. C_{min} was the minimum concentration in the composite profile (Morford et al., 2007).

4. RESULTS

4.1. Sedimentary conditions at the Buzzards Bay site

In order to properly interpret the pore water and solid phase RSM profiles, it is necessary to characterize the conditions in the sediments. Sedimentary conditions that appear to exert control over trace metal mobility include bottom water oxygen concentration, oxygen penetration depth, sedimentary Fe and S cycling, and rates of organic matter oxidation, irrigation and bioturbation (e.g., Barnes and Cochran, 1993; Crusius et al., 1996; Zheng et al., 2000, 2002a; McManus et al., 2005; Aller, 1990, 1994; Canfield et al., 1993a). Therefore, in order to provide the necessary context for our discussion of RSM diagenesis, we will first briefly discuss organic matter oxidation, bioturbation, irrigation and reducing conditions at the Buzzards Bay site.

4.1.1. Organic matter oxidation and sedimentary redox conditions

At the site in Buzzards Bay, TCO_2 is released to pore waters primarily through the oxidation of organic matter, and therefore reflects the rate of organic matter oxidation (McNichol et al., 1988). Although pore water TCO_2 profiles show strong summer/winter and interannual differences, these differences are only weakly reflected in directly

412 measured benthic fluxes (August: 430 ± 40 µmol C/cm^2/y; March: 340 ± 30 µmol
413 C/cm^2/y, n=3; Figures 3A, 3B). The benthic flux of TCO_2 does not vary greatly between
414 these sampling periods; however, the NH_4^+ benthic flux varies from ~ 0 to 50
415 µmol/cm^2/y (Figure 3B). Pore water [NH_4^+] and [TCO_2] are essentially decoupled in
416 March but are closely linked in August with a slope that is consistent with the
417 decomposition of organic matter with Redfield–like stoichiometry. The close correlation
418 between pore water NH_4^+ and TCO_2 concentrations in August indicates that, at those
419 times, sedimentary organic matter decomposition was dominated by anoxic processes
420 that did not lead to NH_4^+ oxidation.

421 Pore water O_2 profiles show a shoaling of the O_2 penetration depth between
422 March 2003 and August 2003, with a concomitant increase in the benthic O_2 flux
423 (March: 410 ± 60 µmol/cm^2/y, n=3; August: 900 ± 100 µmol/cm^2/y, n=3; Figures 3B, 4).
424 The ratio of the O_2:TCO_2 fluxes is 1.2 ± 0.2 in March/April, consistent with the estimate
425 for the oxidation of marine organic matter by O_2 (~1.4, Anderson and Sarmiento, 1994).
426 This result is consistent with recycling and reoxidation of reduced products of organic
427 matter oxidation (e.g., Fe^{2+}, S^{2-}), with O_2 as the ultimate electron acceptor (e.g., Aller,
428 1994). The ratio of the O_2:TCO_2 fluxes is 2.1 ± 0.1 in August; at that time, a significant
429 fraction of O_2 consumption was not linked to concurrent organic matter oxidation.

430 Fe and Mn data show that the site is one where anoxic diagenesis dominates
431 sediments below a thin, oxic cap. Solid phase data (Figure 5) show enrichment of the Fe
432 and Mn in the oxic layer that results from the upward diffusion of dissolved Fe and Mn,
433 followed by oxidation to insoluble oxides. Pore water Fe^{2+} and Mn^{2+} profiles show a
434 strong seasonal progression (Figure 4). The depth of first appearance of dissolved Fe^{2+} is
435 related to the O_2 penetration depth (Figure 4), and the maximum concentrations of Fe^{2+}
436 and Mn^{2+} are related to the rates of Fe and Mn reduction, respectively. We detected no
437 dissolved H_2S in the upper 25 cm of Buzzards Bay pore waters although this does not
438 preclude active sulfate reduction and sulfide production. One possible removal

mechanism for dissolved Fe^{2+} from pore waters is as iron sulfide, and the extent of Fe^{2+} removal may reflect the availability of H_2S for iron sulfide formation. We can then infer more extensive sulfate reduction when we measured lower asymptotic Fe^{2+} concentrations in August 2004. To describe the seasonally variable intensity of reducing conditions, we define "reduction intensity" in sediments with greater reduction intensity reflected by (1) shallower first appearance of dissolved Fe^{2+}, (2) greater maximum dissolved Mn^{2+} and Fe^{2+} concentrations, and (3) lower asymptotic dissolved Fe^{2+} concentration. The order of reduction intensity at the four sampling times is:

March 2003 < April 2001 < August 2003 < August 2004

This ordering of reduction intensity is supported by the variations in O_2 penetration depth.

4.1.2 Particle Mixing

Measurements of excess ^{234}Th and ^{210}Pb in the sediments show solid phase mixing that may contribute to the internal cycle of reduced products of organic matter oxidation (Mn, Fe, and S) and to RSM cycling. Excess ^{234}Th data (Figure 6A) from 0–2 cm suggest that this depth region is dominated by quasi–diffusive mixing, with some evidence of nondiffusive particle transport (see Aug 2003 #1). We measured a single value for the mixing intensity parameter, D_b, of 6 ± 5 cm^2/y in March and widely ranging values of 76, 20 ± 20, and 3 cm^2/y in three August cores. The seasonal variability in rates is similar to that observed at the site by Martin and Sayles (1987), who measured biodiffusion coefficients of 3–10 cm^2/y from December–March (n=3) and 11–25 cm^2/y from July to October (n=4). Excess ^{210}Pb profiles show a surface layer (0–2 cm, Figure 6B) coinciding with the layer of excess ^{234}Th, where the measured D_b of 40 ± 20 cm^2/y is similar to values derived from excess ^{234}Th in the same layer. From 2 to ~5 cm, the average ^{210}Pb profile shows only a small decrease with depth, and there is a more rapid decrease below 5 cm (Figure 6C). Biodiffusion coefficients for both of these deeper layers would exceed the short–term value based on ^{234}Th. It is likely that the ^{210}Pb distribution below 2 cm is dominated by occasional, nondiffusive transport events that homogenize its activity profile over the decadal–scale lifetime of the isotope. In summary, particle mixing at the site is characterized by rapid, quasi–diffusive mixing that

471 is important to processes occurring in the upper ~2 cm on time scales of ~weeks,
472 superimposed on occasional, nonlocal particle transport events.
473
474 *4.1.3 Nondiffusive pore water transport: Irrigation.*
475
476 We consider sediment irrigation to be driven by physical or biological flushing of
477 burrows, coupled with diffusive exchange of solutes between burrows and the
478 surrounding sediment. Solute concentrations in the burrows are assumed to be equal to
479 those in bottom water. If that is the case, irrigation acts to remove solutes from sediments
480 to overlying water when pore water concentrations exceed bottom water values; it acts to
481 add solutes to pore waters when the opposite condition holds (Aller, 1980). The
482 magnitude for each solute depends on its diffusion coefficient (see equations 2 and 3).
483 For this work, we have calculated an average, warm–season (~April–October) α
484 from ^{222}Rn / ^{226}Ra disequilibrium profiles (Martin and Sayles, 1987) and from
485 experiments in which Br^- is added to *in situ* flux chambers as a solute tracer (this work).
486 The distribution of the tracer in pore waters is determined in subcores collected from
487 below the flux chambers at the end of deployments. The data are interpreted using a
488 one–dimensional transport model (Martin and Banta, 1992; Martin and Sayles, 2004).
489 Br^- data and best–fit profiles are shown in Figure 7A. In interpreting the Br^- data, α was
490 assumed to have the depth–dependence:

491
$$x \le L_{max},\ \alpha = \alpha_1 e^{-\alpha_2 x} \quad (7)$$
$$x > L_{max},\ \alpha = 0 \quad (8)$$

492 Best–fit parameter values from the Br^- data are listed along with those from Rn data
493 (Martin and Sayles, 1987; Table 5). There is significant variability in α profiles and no
494 regular, seasonal trend over the April–October time period for these measurements.
495 Therefore, after adjusting the Rn–based measurements for the difference in diffusion
496 coefficients between Br^- and Rn, we calculated an overall, warm–season, average α:

497
$$\alpha_{Br,ave} = 2.957 + 105.51 e^{-0.295 x} \quad (9)$$

498 Based on measurements of both excess Br^- and Rn deficits in pore waters, Buzzards Bay
499 sediments are irrigated to depths of 10–20 cm from April to October (Figure 7B). Based

on ^{222}Rn / ^{226}Ra results, irrigation was absent in December and March (Martin and Sayles, 1987).

4.2. RSM pore water and solid phase profiles

U, Mo, and Re are all removed from pore waters under conditions present in Buzzards Bay sediments (Figure 4). The minimum in pore water concentration extends to the bottom of the pore water profile for Re, but only extends to depths of ~2–7 cm for U and Mo. In the pore waters sampled immediately below the sediment–water interface in March and April, Re release from a solid phase to pore waters above its removal depth is obvious with Re pore water concentrations 1.6–1.9 times greater than its overlying water concentration. Mo release occurs above its removal zone particularly in August 2003. Below its removal zone, U concentrations increase significantly, and with the exception of samples at ~20 cm in August 2004 remain below the bottom water U concentration. Measurements in August 2004 confirmed that pore water U is present in its oxidized form, U(VI), throughout the pore water profile (data not shown) which is consistent with previous research at this location (Cochran et al., 1986). Mo shows the largest increases below 10 cm; at all sampling times, Mo concentrations in deep pore waters increase to values in excess of its bottom water concentration.

The composite solid phase profiles show that there are no surface maxima for U, Re and Mo, and their solid phase profiles increase below the sediment–water interface (Figure 5, Table 6). The solid phase Re gradient deeper than 10 cm is approximately 80% of the gradient shallower than 10 cm, and is consistent with the pore water profiles that show Re removal to the solid phase over the entire sampled sediment depth. The solid phase U and Mo increase linearly over the top 10 cm, with the gradient decreasing to approximately 60% and 30% deeper than 10 cm relative to their shallower gradients, respectively. The area below the zone of removal where pore water U and Mo concentrations increase above their minimum concentrations is coincident with more limited accumulation in the solid phase. To determine the authigenic accumulation rate at the Buzzards Bay site, the authigenic RSM concentrations are calculated from the solid phase profiles (Table 7). The U and Mo accumulation rates are consistent with rates

measured on other continental margins whereas the average Re accumulation rate is generally larger (Table 7; Morford et al., 2007 and references therein).

5. DISCUSSION

5.1. Model results for pore water RSM profiles

To improve our understanding of the RSM pore water profiles and to provide quantitative parameters with which to compare and contrast RSM behavior, the model was fitted to the pore water data. The model uses a depth–invariant first–order rate constant for removal that is determined by fitting the RSM profile. Fitting the entire profile resulted in poor model fits for the data in the removal layer (x_p to x_s) and the data below 10 cm. On the contrary, fits to the data above 10 cm depth were generally excellent when only the shallow data were included. Using this approach, the best–fit value of x_s (the bottom of the removal layer) was just below the depth at which the concentration began to increase. The resultant model–generated pore water profiles provide diffusive fluxes across the sediment–water interface and at depth x_p (F_o and F_{xp}, respectively; Table 8). Below x_s, increases in model RSM concentrations reflect addition to pore waters via irrigation, without any reaction in the sediments. These model profiles deviate from measurements below depth x_s; therefore, fluxes across that depth horizon (F_{xs}) are calculated using linear fits to the pore water profiles around x_s.

With the possible exception of Mo in March 2003, all three RSM are removed from pore waters at all sampling times. The depth at which removal to the solid phase begins varies between the metals, and that for Mo has a strong seasonal dependence. The observed *depth order of onset of removal* (seasonally averaged x_p) of the RSM agrees with the order predicted by the metals' pe^o_{sw}: Re before U before Mo (Table 9). The *extent of removal*, defined here as C_{min}/C_0, shows that both Re and U exhibit greatest removal at the time of maximum reduction intensity (August 2004), and the variability of their extent of removal is relatively small (Table 10). In contrast, the extent of removal of Mo has a strong seasonal dependence. The *maximum depth of removal* (x_s) is similar

for both U and Mo, at ~3–9 cm for all sampling times (Table 8). However, x_s is deeper for Re, which undergoes removal to the solid phase throughout its depth profile in the two August measurements, but not in March 2003 when net removal appears to stop at ~10 cm. The *first order removal rate constants* (k_p) implied by concentration versus depth profiles show no seasonal dependence for Mo and Re; however, the U removal rate constant is much larger in August than in March/April. The overall order for k_p (y^{-1}) is:

U (August, 1260–3400) > Mo (800 ± 400) > U (March/April, 280 ± 40) > Re (100 ± 50)

5.2. Importance of source(s) for authigenic RSM formation in Buzzards Bay sediments

The model results permit the apportionment of RSM removed to authigenic phases among (1) the flux of dissolved metals into the removal zone from bottom water due to both diffusion (F_{xp}) and irrigation (F_{irr}), (2) the input of metals near the sediment–water interface (F_{prod}) due to release of metals from solids to pore waters at depths shallower than x_p, and (3) the flux of dissolved metals from below the removal layer (F_{xs}) which potentially represents an internally cycled component of authigenic metals (Figure 8, Table 11). The rate of metal addition to pore waters above the removal depth, x_p is calculated by:

$$F_{prod} = \phi k_r x_p \qquad (10)$$

The contribution of irrigation to authigenic RSM formation within the zone of authigenic accumulation is calculated over the depth interval from x_p to x_s by:

$$F_{irr,i} = \int_{x_p}^{x_s} \phi \alpha_i (C_{bw} - C_i)\, dx \qquad (11)$$

The flux into the removal layer from below (F_{xs}) is calculated as previously described. Processes occurring deeper than x_s (such as irrigation) are responsible for F_{xs}.

In our steady–state interpretation of metal profiles, the rate of authigenic metal formation is the sum:

$$F_{auth} = F_{xp} + F_{xs} + F_{irr} \qquad (12)$$

In this equation all fluxes are taken to be positive. The authigenic formation rates of U and Mo are lowest at the time of slowest anoxic remineralization but increase steadily as the anoxic remineralization rate increases (Figure 9A). There is no obvious seasonality in the authigenic Re formation rate. The fraction of authigenic metal formation that can be attributed to direct transport from bottom water is

$$f_{bw} = \left[F_{xp} + F_{irr} - \left(F_{prod} - F_{loss}\right)\right] / F_{auth} \quad (13)$$

In this equation F_{loss} is the absolute value of the flux across the sediment–water interface when that flux is directed out of the sediments, as was observed for Mo in August 2003 and for Re in March 2003 and April 2001 (Figure 4). Contributions to authigenic metal formation as a result of the release of RSM from the solid phase to pore waters, either above x_p or below x_s, are not included so as to obtain the best estimate for the fraction of authigenic metal formation due to direct transport from bottom water. The fraction of authigenic metal formation attributable to transport from bottom waters (f_{bw}) may be underestimated since it does not include the contribution of irrigation from F_{xs}, which is non–existent (Re) or small (U) except for Mo. In the case of Mo, F_{xs} includes a contribution from remobilization from the solid phase in addition to any contribution from irrigation (see later discussion).

The U for authigenic phase formation comes almost entirely from dissolved U in bottom water at the Buzzards Bay site (Figure 9B). In contrast, both Re and Mo have other important sources. There is no "recycled" Re: the removal layer for Re extends over most of the sampled layer (Table 8), so there is never an upward Re flux at x_S. However, pore water profiles show an input of Re near the sediment–water interface in March and April, due to release of Re from solids to the dissolved phase. Although some of this apparent Re release may result from sampling artifacts, there is strong evidence for a solid phase source of Re at this site (see next section). Authigenic Mo formation is affected both by release of Mo from the solid phase near the sediment–water interface and by a flux of Mo from below the removal layer ($x > x_S$). Both of these sources increase in intensity from March to August; therefore, sources other than dissolved Mo in bottom water are increasingly important from March to August. Irrigation rate data

indicate that the flux of Mo from below may be supplied partly by irrigation that transports Mo from the water column, but must also include Mo that is remobilized from the solid phase, perhaps by exposure to oxygen as a result of irrigation.

5.3. Benthic chamber RSM fluxes

If small–scale spatial and temporal variability are limited, the benthic fluxes determined with *in situ* chambers at the Buzzards Bay site should equal the sum of diffusive and irrigation–driven fluxes across the sediment–water interface for pore water constituents (Figure 10). Directly measured and calculated U fluxes agreed very well except in March 2003. Pore water RSM modeling results showed that U is the least affected by processes between the sediment–water interface and the removal layer.

Re is strongly affected by near–interface processes in the cold months of March and April. Pore water data show large fluxes out of the sediments at these times. These large, calculated fluxes may be partly due to sampling artifacts that increase the near interface pore water Re concentration (see Figure 10 caption). However, the April Re flux out of sediments is supported by a concurrently measured chamber flux of Re from sediments to overlying water. Calculated Re fluxes into the sediments exceeded directly measured fluxes in August. This difference could again be due to spatial variability or to overestimation of the irrigation flux which assumed no impediments to diffusion across burrow walls.

Like Re, Mo is strongly influenced by near–interface processes, and short–term, small–scale variability may influence flux comparisons. Agreement between chamber and calculated fluxes was reasonable in both August experiments, but less good in March and April. When benthic chambers showed a large outward flux (March) or essentially zero flux (April), pore water fluxes were apparently directed into the sediments.

5.4. A model for RSM diagenesis and accumulation in marine sediments

To obtain a consistent representation of RSM diagenesis in coastal sediments and to form a general model of how RSM accumulate in marine sediments, results from the site in Buzzards Bay are compared to results from a complementary coastal site in Hingham Bay, Massachusetts (Table 1, Figure 1; Morford et al., 2007). We present a

651 general model that is consistent with the experimental–based and field–based literature
652 on RSM geochemistry, and that describes the processes controlling authigenic
653 accumulation in marine sediments (Figure 8).
654 Sites in Hingham and Buzzards bays consistently have high bottom water oxygen
655 concentration throughout the year (~230–380 μM), although the sedimentation rate is
656 more rapid at the Hingham Bay site (Table 1). Hingham Bay has greater organic carbon
657 oxidation rates, which result in slightly shallower oxygen penetration depths during the
658 year (Table 1). Anoxic processes dominate at both sites, which is common along
659 continental margins (e.g., Canfield et al., 1993b; Thamdrup et al., 1994; Boudreau et al.,
660 1998). Differences in the extent of sedimentary anoxic processes between these two sites
661 are apparent by comparing the Fe^{2+}, H_2S and SO_4^{2-} pore water profiles (Figure 11). Both
662 sites have pore water profiles with zones of net release of Fe^{2+} into pore waters below the
663 dissolved Mn^{2+} maximum, but the zone is substantially narrower at Buzzards Bay and the
664 maximum Fe^{2+} concentrations are 25–50% lower at Buzzards Bay at comparable times of
665 year. Below 6 cm at Hingham Bay, TH_2S climbs rapidly to 1000 μM. This rapid rate of
666 sulfate reduction in Hingham Bay is sufficient to completely remove dissolved Fe^{2+},
667 presumably as iron sulfide, and produce high pore water sulfide concentrations. In
668 contrast, in the upper 20 cm at Buzzards Bay there is no measurable H_2S (DL < 2 μM),
669 only a very small SO_4^{2-} depletion, and deep Fe^{2+} concentrations were >10 μmol/kg
670 except in August 2004. These results suggest lower iron and sulfate reduction rates at the
671 site in Buzzards Bay relative to Hingham Bay. A rapidly mixed layer extends 5–6 cm at
672 both sites (this work, Morford et al., 2007). Sediments are well–mixed down to 20–30
673 cm at the Buzzards Bay site (McNichol et al., 1988). The extent of bioturbation, and
674 possibly irrigation, may be limited to the top ~10 cm at the Hingham Bay site due to the
675 presence of high pore water H_2S concentrations below this depth (Benoit et al., 2006).
676
677 *5.4.1. RSM behavior below the sediment–water interface but above the removal zone.*
678
679 The mode of input of RSM to the sediments is important for both the calculation
680 of net fluxes to the solid phase from pore water data and the interpretation of solid phase
681 accumulation rates. The rate of U release (k_r) between the sediment–water interface and

x_p is not important at either location, with only intermittent release of U from sedimentary solids above the zone of removal (Table 8, Figure 8). Re release above x_p is never seen at the Hingham Bay site, and only measured at the Buzzards Bay site during cold months (March and April). Mo is consistently released from sedimentary solids near the sediment–water interface, with the exception of March 2003 at the Buzzards Bay site. The rate of Mo release (k_r) increases in both Hingham and Buzzards bays as reducing conditions increase from winter to early fall.

Benthic chamber experiments in Hingham Bay, where overlying waters were allowed to approach anoxia, showed concurrent release of Mo (and U) with the reduction and dissolution of Mn and/or Fe oxides (Morford et al., 2007). As reducing conditions and the release of Mn and Fe to overlying waters increase, the release of associated Mo from surface sediments also increases. One experiment in April at the site in Buzzards Bay showed a strong release of Re when oxygen was depleted, coincident with Mn release to overlying waters (data not shown). The measured release of Re at only the Buzzards Bay site could be due to the deeper oxygen penetration at this site in the winter (~1 cm) relative to the summer (~0.2 cm). This deeper oxygen penetration may result in the accumulation of Re, providing a reservoir of Re in surface sediments. A shallower oxygen penetration depth would minimize this effect for Re and would be consistent with the absence of Re release between the sediment–water interface and x_p at the Hingham Bay site.

5.4.2. RSM behavior within the removal zone

Consistent features for RSM removal are found in Hingham and Buzzards bays, with the order of onset of removal as Re–U–Mo. The depths of removal (x_p) for Re, U and Mo at the Buzzards Bay site are 0.2 ± 0.3 cm, 0.8 ± 0.6 cm, and 1.8 ± 0.4 cm, respectively, whereas removal begins at 0 cm, 0.9 ± 0.8 cm, and 4 ± 1 cm, respectively, at the Hingham Bay site. The depth of removal for Mo is deeper and deepens with increasing reducing conditions (January to October) at the Hingham Bay site. In contrast, at the Buzzards Bay site x_p is shallower and shoals from April to August. The extent of removal (C_{min}/C_0) is seasonally variable for Mo at both sites, with more extensive removal during periods of greater reducing conditions (Table 10). At the Hingham Bay

site, Mo is the most extensively removed of the three RSM, whereas it is the least extensively removed at the Buzzards Bay site (Table 10). These differences for Mo are due to the balance between Fe and sulfate reduction at the two sites. It seems likely that Mo removal from pore water requires the presence of pore water sulfide, perhaps in microenvironments (e.g., Helz et al., 1996). The zones of iron oxide and sulfate reduction in sediments overlap, leading to removal of H_2S at the Buzzards Bay site in the presence of pore water Fe^{2+} via the formation of FeS. The slower Fe reduction at the Buzzards Bay site results in pore water sulfide consuming Fe^{2+} and resulting in low levels of pore water sulfide that increase as reducing conditions increase. These conditions result in the more limited removal of Mo from pore waters at shallower depths, with depths becoming progressively shallower as reducing conditions intensify. The significantly higher Fe reduction rate in October in Hingham Bay, as denoted by the largest measured pore water Fe^{2+} (Figure 11), results in greater consumption of pore water sulfide and a correspondingly deeper removal depth for Mo. The ultimate extent of removal at the Hingham Bay site is correspondingly much greater, presumably due to the formation of thiomolybdates and their irreversible removal to the solid phase (Bostick et al., 2003).

At both sites, the removal rate (k_p, Table 8) is lowest for Re, and there is a lack of obvious seasonality in both its removal rate and its authigenic formation (Figure 9A). This lack of seasonality suggests an abiotic removal mechanism for Re. Re is present at extremely low pore water concentrations, which may contribute to its limited biological usefulness. In contrast, seasonal increases in authigenic U and Mo formation are obvious with increasing anoxic remineralization rates. The balance between iron and sulfate reduction and the resulting formation of sulfidic microenvironments drives authigenic Mo formation. The additional seasonality of the U removal rate (k_p) in Buzzards Bay is consistent with microbially mediated reduction that is most intense during August, the time of greatest reduction intensity.

5.4.3. The effect of irrigation and RSM behavior below the removal zone

744 In addition to enhancing exchange between bottom water and pore waters,
745 irrigation can transport O_2 from bottom water to O_2–depleted pore waters. In this way,
746 sediments that are removed from the sediment–water interface can be exposed to O_2,
747 potentially resulting in RSM remobilization from the solid phase. All three RSM reach
748 constant, asymptotic pore water concentrations at the site in Hingham Bay (Morford et
749 al., 2007). In Buzzards Bay, Re also reaches a constant, asymptotic pore water
750 concentration and is removed over almost the entire depth range of sampled sediments.
751 Removal of pore water Re throughout the sampled depth results in steadily increasing
752 solid phase Re concentrations (Figure 12). Thus, the model predicts that any Re that is
753 added by irrigation is removed to the solid phase. If that is the case, then irrigation
754 enhances authigenic Re accumulation at the Buzzards Bay site. The solid phase Re
755 profile from Hingham Bay is consistent with a removal zone that only extends through
756 the non–sulfidic zone (Figure 12), due to the absence of irrigation within the sulfidic zone
757 (Benoit et al., 2006).
758 In all cases at the Buzzards Bay site, pore water U increases below the removal
759 layer, consistent with previous U measurements in this area (Cochran et al., 1986).
760 Except in August 2004, pore water U remains below the bottom water concentration; this
761 result is consistent with addition of U by irrigation and subsequent upward diffusion of U
762 to the removal layer where it is removed (Figure 8). It is possible that U is remobilized to
763 some extent by the input of O_2 but the pore water profiles only show the net effect of
764 possible processes: addition via irrigation and remobilization from the solid phase.
765 Below the net removal layer at Buzzards Bay, pore water Mo increases above its
766 bottom water concentration. Therefore, Mo must be remobilized at depth, perhaps as a
767 result of exposure of O_2–deficient sediments to O_2 through irrigation. Because deep Mo
768 concentrations exceed the bottom water concentration, irrigation tends to remove Mo
769 from sediments to overlying water. Remobilization of recently formed authigenic Mo
770 appears to limit its solid phase accumulation at this site. It is also possible that the
771 presence of high pore water sulfide concentrations results in more stable Mo phases in
772 Hingham Bay. Based on the pore water sulfide concentrations at the Hingham Bay site
773 and the lack of measurable sulfide at the Buzzards Bay site, aqueous Mo is most likely
774 present in deep pore waters as MoO_4^{2-} in Buzzards Bay and as MoS_4^{2-} in Hingham Bay

(Helz et al., 2004). Molybdate is less effectively scavenged and only weakly and reversibly retained on pyrite relative to tetrathiomolybdate (Bostick et al., 2003), which would explain the easy return of Mo to pore waters below its removal depth at the Buzzards Bay site.

Although there is a good correlation between the benthic fluxes and authigenic accumulation rates of U and Mo at Hingham Bay (Morford et al., 2007), our results at the Buzzards Bay site are consistent with irrigation ultimately resulting in the partial loss of U and Mo from the solid phase. This difference between the locations is presumably due to the deeper irrigation that occurs at the Buzzards Bay site. At the Buzzards Bay site, the solid phase U and Mo accumulation rates are 20–30% of the modeled flux of authigenic metal formation that can be attributable to direct transport from bottom waters (Table 7). The solid phase accumulation rate and the modeled flux for Re are similar within the uncertainties of our measurements. Irrigation augments Re accumulation but it does not appear to compromise its accumulation in sediments. Our sampling overemphasizes the importance of warm season fluxes. However, our comparison of modeled fluxes and measured accumulation rates indicates the importance of irrigation to augment (Re, possibly U) or compromise (Mo, U) authigenic accumulation in sediments.

6. CONCLUSIONS

Our comprehensive seasonal research at a site in Buzzards Bay identifies the mobilization and immobilization processes in sediments that must be considered in order to understand authigenic accumulation of RSM in coastal sediments. Our results from Buzzards Bay, which has non-measureable pore water sulfide, are compared with previous research from a site with sulfidic pore waters (Hingham Bay). This comparison results in a consistent description of RSM diagenesis in marine sediments.

RSM diagenesis in sediments can be defined in three distinct zones: above the zone of removal, within the zone of removal, and below the zone of removal. Release of RSM to pore waters during the remineralization of solid phases may occur at shallower depths above the zone of authigenic RSM formation. Mo is consistently released from shallow sediments at both sites, but U release only occurs intermittently and Re release was only measured during the cold months in Buzzards Bay. Mo release from surface

807 sediments is greater under more reducing conditions, and is associated with the reduction
808 and remobilization of Mn and/or Fe oxides. The measured release of Re at only the
809 Buzzards Bay site could be due to the deeper oxygen penetration at this site in the winter,
810 which may result in the production of a reservoir of Re in surface sediments. With our
811 results, we cannot discern whether solids are deposited from the water column or
812 recycled in the sediments via remobilization near the interface.
813 There is a consistent order of removal at both locations, with the onset of removal
814 following the order Re–U–Mo. At the Buzzards Bay site, the removal zone for pore
815 water Re extends to the bottom of the profile. The rate of authigenic Re formation and its
816 modeled removal rate from pore waters are independent of the rate of anoxic
817 mineralization, suggesting an abiotic pathway for Re accumulation in sediments. At the
818 Buzzards Bay site, the zone of removal is restricted to ~2–9 cm for U and Mo. For U,
819 both the removal and authigenic formation rates in Buzzards Bay are seasonally
820 dependent and consistent with microbially mediated reduction that is most intense during
821 the times of greater reduction intensity. The increase in authigenic Mo formation with
822 increasing anoxic remineralization may be related to the balance between iron and sulfate
823 reduction rates, and the formation of sulfidic microenvironments. Slow iron and sulfate
824 reduction rates at the Buzzards Bay site produce pore water Fe^{2+} that can consume pore
825 water sulfide by producing FeS phases; a seasonal intensification of reducing conditions
826 then results shallower consumption of Fe^{2+} and the formation of sulfidic
827 microenvironments suitable for limited pore water Mo removal. At the Hingham Bay
828 site, greater iron reduction rates lead to the consumption of pore water sulfide over a
829 larger depth range, so that the appearance of pore water sulfide and the resulting
830 extensive removal of pore water Mo only occur deeper in the sediments.
831 Processes that occur below the zone of removal also ultimately affect the
832 accumulation of RSM in sediments. Pore water Re, U and Mo reach constant, asymptotic
833 concentrations in sulfidic sediments, where irrigation appears to be limited to the shallow,
834 non–sulfidic pore waters. At Buzzards Bay, where irrigation extends 10–20 cm, pore
835 water Re also reaches an asymptotic pore water concentration, whereas pore water U and
836 Mo concentrations increase below their removal zones. Any Re that is added by
837 irrigation is removed to the solid phase, thereby augmenting its authigenic accumulation.

The increases in pore water U concentrations are consistent with the addition of U by irrigation. However, simple addition of Mo via irrigation cannot explain deep pore water Mo concentrations that exceed its bottom water concentrations. Remobilization of Mo from the solid phase to pore waters due to oxidation via nondiffusive transport of oxygen to deep sediments is required to explain the Mo pore water profiles. The comparison between solid phase profiles and RSM fluxes into the removal zone suggest that reoxidation of U and Mo on short timescales is an important process in determining the ultimate accumulation rates in continental margin sediments with non–detectable pore water sulfide. The importance of irrigation and whether it augments (Re, possibly U) or compromises (U, Mo) authigenic accumulation appears to be tied to the depth dependence of irrigation and is related to the presence or absence of pore water sulfide.

Acknowledgements The authors would like to thank the captains of the *Asterias* and *Tioga* and for their help with sample collection. WHOI divers, and Lary Ball in particular, provided valuable field assistance. The authors would also like to thank Joanne Goudreau (WHOI) who was indispensable during benthic chamber preparation, deployment and recovery, and who carried out many chemical analyses. JLM acknowledges the ICP–MS expertise provided by Joanne Goudreau and Dave Schneider (WHOI Plasma Facility). Isotope spikes were generously provided by Bernhard Peucker–Ehrenbrink (^{185}Re) and Greg Ravizza (^{95}Mo). Linda Kalnejais, Ida–Maja Karle, Katherine Watson and F&M undergraduates Melissa Reinard, Sarah Gallagher, Gloria Yen and Elizabeth Herrle provided essential assistance during fieldwork. Yoana Voynova (F&M) provided early insight on this project. Carol Strausser, Lisa Mertzman and Steve Sylvester provided valuable support and assistance at F&M. The authors appreciate the thorough comments of the associate editor, Dr. Tim Shaw, and an anonymous reviewer. The authors also acknowledge financial support from the National Science Foundation (JLM, WRM: OCE–0220892), Research Corporation (JLM, CMC), Franklin & Marshall College, and the Hackman Summer Research Program at F&M.

867 **References**

868 Adelson J. M., Helz G. R. and Miller C. V. (2001) Reconstructing the rise of recent
869 coastal anoxia; molybdenum in Chesapeake Bay sediments. *Geochim. Cosmochim.*
870 *Acta* **65**(2), 237-252.
871 Algeo T. J. and Lyons T. W. (2006) Mo-total organic carbon covariation in modern
872 anoxic marine environments: Implications for analysis of paleoredox and
873 paleohydrographic conditions. *Paleoceanography* **21**(doi: 10.1029/2004PA001112).
874 Aller R. C. (1990) Bioturbation and manganese cycling in hemipelagic sediments. *Phil.*
875 *Trans. Roy. Soc. London A* **331**, 51-68.
876 Aller R. C. (1994) The sedimentary Mn cycle in Long Island Sound: Its role as
877 intermediate oxidant and the influence of bioturbation, O_2, and C_{org} flux on
878 diagenetic reaction balances. *Journal of Marine Research* **52**, 259-295.
879 Anbar A. D., Creaser R. A., Papanastassiou D. A. and Wasserburg G. J. (1992) Rhenium
880 in seawater: Confirmation of generally conservative behavior. *Geochim.*
881 *Cosmochim. Acta* **56**, 4099-4103.
882 Anderson R. F. (1982) Concentration, vertical flux, and remineralization of particulate
883 uranium in seawater. *Geochim. Cosmochim. Acta* **46**, 1293-1299.
884 Anderson L. A. and Sarmiento J. L. (1994) Redfield ratios of remineralization determined
885 by nutrient data analysis. *Global Biogeochemical Cycles* **8**(1), 65-80.
886 Anderson R. F., LeHuray A. P., Fleisher M. Q. and Murray J. W. (1989) Uranium
887 deposition in Saanich Inlet sediments, Vancouver Island. *Geochim. Cosmochim.*
888 *Acta* **53**, 2205-2213.
889 Anderson R. F., Kumar N., Mortlock R. A., Froelich P. N., Kubik P., Dittrich-Hannen B.
890 and Suter M. (1998). Late-Quaternary changes in productivity of the Southern
891 Ocean. *Journal of Marine Systems* **17**, 497-514.
892 Andrews D. and Bennett A. (1981) Measurements of diffusivity near the sediment-water
893 interface with a fine-scale resistivity probe. *Geochim. Cosmochim. Acta* **45**, 2169-
894 2175.
895 Banta G. T. (1991) Decomposition and nitrogen cycling in coastal marine sediments –
896 controls by temperature, organic matter inputs, and benthic macrofauna. PhD.
897 Thesis, Boston University.
898 Barnes C. E. and Cochran J. K. (1991) Geochemistry of uranium in Black Sea sediments.
899 *Deep-Sea Res.* **38**(2), S1237-S1254.
900 Barnes C. E. and Cochran J. K . (1993) Uranium geochemistry in estuarine sediments:
901 Controls on removal and release processes. *Geochim. Cosmochim. Acta* **57**, 555-569.
902 Benoit J. M., Shull D. H., Robinson P. and Ucran L. R. (2006) Infaunal burrow densities
903 and sediment monomethyl mercury distributions in Boston Harbor, Massachusetts.
904 *Mar. Chem.* **102**(1-2), 124-133.
905 Berner R. A. (1980) *Early Diagenesis: A Theoretical Approach*. Princeton University
906 Press, Princeton, NJ.
907 Bertine K. K. and Turekian K. (1973) Mo in marine deposits. *Geochim. Cosmochim. Acta*
908 **37**, 1415-1434.
909 Bostick, B. C., Fendorf S. and Helz G. R. (2003) Differential Adsorption of Molybdate
910 and Tetrathiomolybdate on Pyrite (FeS_2). *Environ. Sci. Technol*. **37**, 285-291.

911 Bothner M. H., Buchholtz ten Brink M. and Manheim F. T. (1998) Metal concentrations
912 in surface sediments of Boston Harbor–Changes with time. *Marine Environmental*
913 *Research* **45**(2), 127-155.
914 Boudreau B. P. (1984) On the equivalence of nonlocal and radial-diffusion models for
915 porewater irrigation. *Journal of Marine Research* **42**, 731-735.
916 Boudreau B. P., Mucci A., Sundby B., Luther G. W. and Silverberg N. (1998)
917 Comparative diagenesis at three sites on the Canadian continental margin. *Journal of*
918 *Marine Research* **56**, 1259-1284.
919 Breckel E. J., Emerson S. and Balistrieri L. (2005) Authigenesis of trace metals in
920 energetic tropical shelf environments. *Continental Shelf Research* **25**, 1321-1337.
921 Brownawell B. (1986) The role of colloidal organic matter in the marine geochemistry of
922 PCBs. Ph. D. dissertation, WHOI/MIT.
923 Calvert S. E. and Pedersen T. F. (1993) Geochemistry of recent oxic and anoxic marine
924 sediments: Implications for the geological record. *Marine Geology* **113**, 67-88.
925 Canfield D. E., Thamdrup B. and Hansen J. W. (1993a) The anaerobic degradation of
926 organic matter in Danish coastal sediments: Iron reduction, manganese reduction,
927 and sulfate reduction. *Geochim. Cosmochim. Acta* **57**, 3867-3883.
928 Canfield D. E., Jorgensen B. B., Fossing H., Glud R., Gundersen J., Ramsing N. B.,
929 Thamdrup B., Hansen J. W., Nielsen L. P. and Hall P. O. J. (1993b) Pathways of
930 organic carbon oxidation in three continental margin sediments. *Marine Geology*
931 **113**, 27-40.
932 Chaillou G., Anschutz P., Lavaux G., Schäfer J. and Blanc G. (2002) The distribution of
933 Mo, U, and Cd in relation to major redox species in muddy sediments of the Bay of
934 Biscay. *Mar. Chem.* **80**, 41-59.
935 Chase Z., Anderson R. F. and Fleisher M. Q. (2001) Evidence from authigenic uranium
936 for increased productivity of the glacial Subantarctic Ocean. *Paleoceanography*
937 2000PA000542.
938 Christensen J. P., Devol A. H., Smethie W. M. (1984) Biological enhancement of solute
939 exchange between sediments and bottom water on the Washington continental shelf.
940 *Continental Shelf Research* **3**, 9-23.
941 Church T. M., Sarin M. M., Fleisher M. Q. and Ferdelman T. G. (1996) Salt marshes: An
942 important coastal sink for dissolved uranium. *Geochim. Cosmochim. Acta* **60**(20),
943 3879-3887.
944 Cline J. (1969) Spectrophotometric determination of hydrogen sulfide in natural waters.
945 *Limnol. Oceanogr*. **14**(3), 454-458.
946 Cochran J. K., Carey A. E., Sholkovitz E. R. and Surprenant L. D. (1986) The
947 geochemistry of uranium and thorium in coastal marine sediments and sediment pore
948 water. *Geochim. Cosmochim. Acta* **50**, 663-680.
949 Collier R. W. (1985) Molybdenum in the Northeast Pacific Ocean. *Limnol. Oceanogr*. **30**,
950 1351-1353.
951 Colodner D., Sachs J., Ravizza G., Turekian K., Edmond J. and Boyle E. (1993) The
952 geochemical cycle of rhenium: a reconnaissance. *Earth Planet. Sci. Lett*. **117**, 205-
953 221.
954 Crusius J. and Thomson J. (2000) Comparative behavior of authigenic Re, U, and Mo
955 during reoxidation and subsequent long-term burial in marine sediments. *Geochim.*
956 *Cosmochim. Acta* **64**(13), 2233-2242.

957 Crusius J., Calvert S., Pedersen T. and Sage D. (1996) Rhenium and molybdenum
958 enrichments in sediments as indicators of oxic, suboxic and sulfidic conditions of
959 deposition. *Earth Planet. Sci. Lett*. **145**, 65-78.
960 Dean W. E., Gardner J. V. and Piper D. Z. (1997) Inorganic geochemical indicators of
961 glacial-interglacial changes in productivity and anoxia on the California continental
962 margin. *Geochim. Cosmochim. Acta* **61**(21), 4507-4518.
963 Dean W. E., Piper D. Z. and Peterson L. C. (1999) Molybdenum accumulation in Cariaco
964 basin sediment over the past 24 k.y.: A record of water-column anoxia and climate.
965 *Geology* **27**(6), 507-510.
966 Duff M. C., Coughlin J. U. and Hunter D. B. (2002) Uranium co-precipitation with iron
967 oxide minerals. *Geochim. Cosmochim. Acta* **66**(20), 3533-3547.
968 Emerson S. R. and Huested S. S. (1991) Ocean anoxia and the concentrations of
969 molybdenum and vanadium in seawater. *Mar. Chem.* **34**, 177-196.
970 Emerson S. R., Jahnke R., and Heggie D. (1984) Sediment-water exchange in shallow
971 water estuarine sediments. *Journal of Marine Research* **42**, 709-730.
972 Erickson B. E. and Helz G. R. (2000) Molybdenum(VI) speciation in sulfidic waters:
973 Stability and lability of thiomolybdates. *Geochim. Cosmochim. Acta* **64**(7), 1149-
974 1158.
975 Francis A. J., Dodge C. J., Lu F., Halada G. P. and Clayton C. R. (1994) XPS and
976 XANES studies of uranium reduction by *Clostridium* sp. *Environ. Sci. Technol.* **28**,
977 636-639.
978 François R., Altabet M. A., Yu E.-F., Sigman D. M., Bacon M. P., Frank M., Bohrmann
979 G., Bareille G. and Labeyrie L. D. (1997) Contribution of Southern Ocean surface-
980 water stratification to low atmospheric CO_2 concentrations during the last glacial
981 period. *Nature* **389**, 929-935.
982 Glibert P. L. and Loder T. C. (1977) Automated analysis of nutrients in seawater: A
983 manual of techniques. Technical Report, Woods Hole Oceanographic Institution,
984 Woods Hole, MA.
985 Helz G. R., Miller C. V., Charnock J. M., Mosselmans J. F. W., Pattrick R. A. D., Garner
986 C. D. and Vaughan D. J. (1996) Mechanism of molybdenum removal from the sea
987 and its concentration in black shales: EXAFS evidence. *Geochim. Cosmochim. Acta*
988 **60**(19), 3631-3642.
989 Helz G. R., Vorlicek T. P. and Kahn M. D. (2004) Molybdenum scavenging by iron
990 monosulfide. *Environ. Sci. Technol*. **38**, 4263-4268.
991 Kalnejais L. H. (2005). Mechanisms of Metal Release from Contaminated Coastal
992 Sediments, Massachusetts Institute of Technology/Woods Hole Oceanographic
993 Institution**:** 238.
994 Kato Y., Tanase M., Minami H. and Okabe S. (1995) Remobilization of transition
995 elements in pore water of continental slope sediments. In *Biogeochemical Processes*
996 *and Ocean Flux in the Western Pacific* (eds. H. Sakai and Y. Nozaki), Terra
997 Scientific Publishing, pp 383-405.
998 Klinkhammer G. P. and Palmer M. R. (1991) Uranium in the oceans: Where it goes and
999 why. *Geochim. Cosmochim. Acta* **55**, 1799-1806.
1000 Koide M., Hodge V. F., Yany J., Stallard M., Goldberg E., Calhoun J. and Bertine K.
1001 (1986) Some comparative marine geochemistries of rhenium, gold, silver and
1002 molybdenum. *Appl. Geochim.* **1**, 705-714.

1003 Ku, T. L., Knauss K. G., and Mathieu G. G. (1977) Uranium in the open ocean:
1004 concentration and isotopic composition. *Deep-Sea Res.* **24**, 1005-1017.
1005 Li Y. and Gregory S. (1974) Diffusion of ions in sea water and in deep-sea sediments.
1006 *Geochim. Cosmochim. Acta* **38**, 703-714.
1007 Lovley D. R., Phillips E. J. P., Gorby Y. A. and Landa E. R. (1991) Microbial reduction
1008 of uranium. *Nature* **350**, 413-416.
1009 Manheim F. T., Dwight L. and Belastock R. A. (1974) Porosity, density, grain density,
1010 and related physical properties of sediments from the Red Sea drill cores. In *Initial*
1011 *Reports of the Deep Sea Drilling Project XXIII. v. 42, part 2* (eds. R. B. Whitmarsh,
1012 D. A. Ross) pp 887-907.
1013 Martin W.R. and Banta G. T. (1992) The measurement of sediment irrigation rates: A
1014 comparison of the Br^- tracer and $^{222}Rn/^{226}Ra$ disequilibrium techniques. *Journal of*
1015 *Marine Research* **50**, 125-154.
1016 Martin W. R. and Sayles F. L. (1987) Seasonal cycles of particle and solute transport
1017 processes in nearshore sediments: $^{222}Rn/^{226}Ra$ and $^{234}Th/^{238}U$ disequilibrium at a site
1018 in Buzzards Bay, MA. *Geochim. Cosmochim. Acta* **51**, 927-943.
1019 Martin W. R. and Sayles F. L. (2004) Organic matter cycling in sediments of the
1020 continental margin in the northwest Atlantic Ocean. *Deep-Sea Research I* **51**, 457-
1021 489.
1022 Mas J. L., Tagami K. and Uchida S. (2005) Rhenium measurements on North Atlantic
1023 seaweed samples by ID-ICP-MS: An observation on the Re concentration factors.
1024 *Journal of Radioanalytical and Nuclear Chemistry* **265**(3), 361-365.
1025 McDuff R. E. and Ellis R. A. (1979) Determining diffusion coefficients in marine
1026 sediments: a laboratory study of the validity of resistivity techniques. *American*
1027 *Journal of Science* **279**, 666-675.
1028 McKee B. A., DeMaster D. J., Nittrouer C. A. (1987) Uranium geochemistry on the
1029 Amazon shelf: Evidence for uranium release from bottom sediments. *Geochim.*
1030 *Cosmochim. Acta* **51**, 2779-2786.
1031 McManus J., Berelson W. M., Klinkhammer G. P., Hammond D. E. and Holm C. (2005)
1032 Authigenic uranium: relationship to oxygen penetration depth and organic carbon
1033 rain. *Geochim. Cosmochim. Acta* **69**(1), 95-108.
1034 McManus J., Berelson W. M., Severmann S., Poulson R. L., Hammond D. E.,
1035 Klinkhammer G. P. and Holm C. (2006) Molybdenum and uranium geochemistry in
1036 continental margin sediments: Paleoproxy potential. *Geochim. Cosmochim. Acta*
1037 doi:10.1016/j.gca.2006.06.1564.
1038 McNichol A. P., Lee C., and Druffel E. R. M. (1988) Carbon cycling in coastal
1039 sediments: 1. A quantitative estimate of the remineralization of organic carbon in the
1040 sediments of Buzzards Bay, MA. *Geochim. Cosmochim. Acta* **52**, 1531-1543.
1041 Meyers S. R., Sageman B. B. and Lyons T. W. (2005) Organic carbon burial rate and the
1042 molybdenum proxy: Theoretical framework and application to Cenomanian-
1043 Turonian oceanic anoxic event 2. *Paleoceanography* **20**(doi:
1044 10.1029/2004PA001068).
1045 Moore J.R. (1963) Bottom sediment studies, Buzzards Bay, Massachusetts. J.
1046 *Sedimentary Petrology* **33**(3), 511-558.
1047 Morford J. L and Emerson S. (1999) The geochemistry of redox sensitive trace metals in
1048 sediments. *Geochim. Cosmochim. Acta* **63**, 1735-1750.

1049 Morford J. L., Kalnejais L., Martin W., Francois R. and Karle I.-M. (2003) Sampling
1050 marine pore waters for Mn, Fe, U, Re and Mo: modifications on diffusional
1051 equilibration thin film gel probes. *Journal of Experimental Marine Biology and*
1052 *Ecology* **285-286**, 85-103.
1053 Morford J. L., Emerson S. R., Breckel E. J. and Kim S. H. (2005) Diagenesis of
1054 oxyanions (V, U, Re, and Mo) in pore waters and sediments from a continental
1055 margin. *Geochim. Cosmochim. Acta* **69**(21), 5021-5032.
1056 Morford J. L., Martin W.R., Kalnejais L., Francois R., Bothner M. and Karle I.-M. (2007)
1057 Insights on geochemical cycling of U, Re and Mo from seasonal sampling in Boston
1058 Harbor, Massachusetts, U.S.A. *Geochimica et Cosmochimica Acta* **71**(4), 895-917.
1059 Murray R. W. and Leinen M. (1993) Chemical transport to the seafloor of the Equatorial
1060 Pacific Ocean across a latitudinal transect at 135°W: Tracking sedimentary major,
1061 trace and rare earth element fluxes at the Equator and the Intertropical Convergence
1062 Zone. *Geochim. Cosmochim. Acta* **57**(17), 4141-4163.
1063 Nameroff T. J., Balistrieri L. S. and Murray J. W. (2002) Suboxic trace metal
1064 geochemistry in the eastern tropical North Pacific. *Geochim. Cosmochim. Acta*
1065 **66**(7), 1139-1158.
1066 Nameroff T. J., Calvert S. E. and Murray J. W. (2004) Glacial-interglacial variability in
1067 the eastern tropical North Pacific oxygen minimum zone recorded by redox-sensitive
1068 trace metals. *Paleoceanography* **19**, doi: 10.1029/2003PA000912
1069 Nigrini A. (1970) Diffusion in rock alteration systems: I. Prediction of limiting equivalent
1070 ionic conductances at elevated temperatures. *American Journal of Science* **269**, 65-
1071 91.
1072 O'Sullivan D. W. and Millero F. J. (1998) Continual measurement of the total inorganic
1073 carbon in surface seawater. *Mar. Chem.* **60**, 75-83.
1074 Piper D. Z. (1994) Seawater as the source of minor elements in black shales, phosphorites
1075 and other sedimentary rocks. *Chemical Geology* **114**, 95-114.
1076 Rodushkin I. and Ruth T. (1997) Determination of trace metals in estuarine and seawater
1077 reference materials by high resolution inductively coupled plasma mass spectrometry.
1078 *J. Anal. At. Spectrom.* **12**, 1181-1185.
1079 Roman M. R. and Tenore K. R. (1978) Tidal resuspension in Buzzards Bay,
1080 Massachusetts I. Seasonal changes in the resuspension of organic carbon and
1081 chlorophyll a. *Estuarine and Coastal Marine Science* **6**, 37-46.
1082 Rosenfeld L. K., Signell R. P. and Gawarkiewicz G. (1984) Hydrographic Study of
1083 Buzzards Bay, 1982-1983. WHOI Technical Report #WHOI-84-5.
1084 Rosenthal Y., Boyle E. A., Labeyrie L., and Oppo D. (1995) Glacial enrichments of
1085 authigenic Cd and U in Subantarctic sediments: A climatic control on the elements'
1086 ocean budget? *Paleoceanography* **10,** 395-413.
1087 Rowe G. T. and McNichol A. P. (1991) Carbon cycling in coastal sediments: Estimating
1088 remineralization in Buzzards Bay, Massachusetts. *Geochim. Cosmochim. Acta* **55**,
1089 2989-2991.
1090 Sanders, H. L. (1958) Benthic studies in Buzzards Bay. I. Animal-sediment relationships.
1091 *Limnol. Oceanogr*. **3**(3), 245-258.
1092 Sani R. K., Peyton B. M., Amonette J. E. and Geesey G. G. (2004) Reduction of
1093 uranium(VI) under sulfate-reducing conditions in the presence of Fe(III)-
1094 (hydro)oxides. *Geochim. Cosmochim. Acta* **68**(12), 2639-2648.

1095 Sayles F. L. and Dickinson W. H. (1991) The ROLAI2D lander: a benthic lander for the
1096 study of exchange across the sediment-water interface. *Deep-Sea Research* **38**(5),
1097 505-529.
1098 Sayles F. L. and Martin W. R. (1995) *In situ* tracer studies of solute transport across the
1099 sediment-water interface at the Bermuda Time Series site. *Deep-Sea Research I* **42**,
1100 31-52.
1101 Sayles F. L., Martin W. R., Chase Z. and Anderson R. F. (2001) Benthic remineralization
1102 and burial of biogenic SiO_2, $CaCO_3$, organic carbon, and detrital material in the
1103 Southern Ocean along a transect at 170° West. *Deep-Sea Research II* **48**, 4323-4383.
1104 Senko J. M., Istok J. D., Suflita J. M. and Krumholz L. R. (2002) *In-situ* evidence for
1105 uranium immobilization and remobilization. *Environ. Sci. Technol*. **36**, 1491-1496.
1106 Shaw T. J., Gieskes J. M. and Jahnke R. A. (1990) Early diagenesis in differing
1107 depositional environments: The response of transition metals in pore water.
1108 *Geochim. Cosmochim. Acta* **54** 1233-1246.
1109 Shaw T. J., Sholkovitz E. R. and Klinkhammer G. (1994) Redox dynamics in the
1110 Chesapeake Bay: the effect on sediment/water uranium exchange. *Geochim.*
1111 *Cosmochim. Acta* **58**(14), 2985-2995.
1112 Sundby B., Martinez P. and Gobeil C. (2004) Comparative geochemistry of cadmium,
1113 rhenium, uranium, and molybdenum in continental margin sediments. *Geochim.*
1114 *Cosmochim. Acta* **68**(11), 2485-2493.
1115 Thamdrup B., Fossing H. and Jorgensen B. B. (1994) Manganese, iron, and sulfur cycling
1116 in a coastal marine sediment, Aarhus Bay, Denmark. *Geochim. Cosmochim. Acta*
1117 **58**(23), 5115-5129.
1118 Tribovillard N., Algeo T. J., Lyons T. and Riboulleau A. (2006) Trace metals as
1119 paleoredox and paleoproductivity proxies: An update. *Chemical Geology* **232**, 12-32.
1120 Tucker M. D., Barton L. L. and Thomson B. M. (1996) Kinetic coefficients for
1121 simultaneous reduction of sulfate and uranium by *Desulfovibrio desulfuricans*. *Appl.*
1122 *Microbiol. Biotechnol.* **46**, 74-77.
1123 Turekian K. K. and Wedepohl K. H. (1961) Distribution of the elements in some major
1124 units of the earth's crust. *Geol. Soc. Amer. Bull.* **72**, 175-192.
1125 Vorlicek T. P. and Helz G. R. (2002) Catalysis by mineral surfaces: Implications for Mo
1126 geochemistry in anoxic environments. *Geochim. Cosmochim. Acta* **66**(21), 3679-
1127 3692.
1128 Vorlicek T. P., Kahn M. D., Kasuya Y. and Helz G. R. (2004) Capture of molybdenum in
1129 pyrite-forming sediments: Role of ligand-induced reduction by polysulfides.
1130 *Geochim. Cosmochim. Acta* **68**(3), 547-556.
1131 Wharton M. J., Atkins B., Charnock J. M., Livens F. R., Pattrick R. A. D., and Collison
1132 D. (2000) An x-ray absorption spectroscopy study of the coprecipitation of Tc and
1133 Re with mackinawite (FeS). *Applied Geochemistry* **15**, 347-354.
1134 Yamashita Y., Takahashi Y., Haba H., Enomoto S. and Hiroshi S. (2007) Comparison of
1135 reductive accumulation of Re and Os in seawater – sediment systems. *Geochim.*
1136 *Cosmochim. Acta* **71**, 3458-3475.
1137 Yang J. S. (1991) High rhenium enrichment in brown algae: A biological sink of rhenium
1138 in the sea? *Hydrobiologia* **211**, 165-170.

1139 Zheng Y., Anderson R. F., van Geen A. and Kuwabara J. (2000) Authigenic molybdenum
1140 formation in marine sediments: A link to pore water sulfide in the Santa Barbara
1141 Basin. *Geochim. Cosmochim. Acta,* **64**(24), 4165-4178.
1142 Zheng Y., Anderson R. F., van Geen A. and Fleisher M. Q. (2002a) Remobilization of
1143 authigenic uranium in marine sediments by bioturbation. *Geochim. Cosmochim.*
1144 *Acta*, **66**(10), 1759-1772.
1145 Zheng Y., Andeson R. F., van Geen A. and Fleisher M. Q. (2002b) Preservation of
1146 particulate non-lithogenic uranium in marine sediments. *Geochim. Cosmochim. Acta*,
1147 **66**(17), 3085-3092.
1148
1149

Figure Captions

Figure 1. Map of the sampling sites in Buzzards Bay and Hingham Bay, Massachusetts, off the northeastern coast of the U.S.A.

Figure 2. Plots of (A) porosity and (B) log {porosity} versus log {1/F}, where the formation factor (F) is the ratio of sediment resistivity to that of pore water (McDuff and Ellis, 1979) for the site in Buzzards Bay. The slope of the linear regression in plot (B) is ν (see Table 4).

Figure 3. Buzzards Bay pore water profiles and benthic chamber fluxes. (A) Plots of pore water ammonium and TCO_2 show strong summer/winter and interannual differences. The horizontal and vertical lines denote the standard deviations for the average concentrations, where the average concentrations are determined from either two or three cores. There are no TCO_2 measurements in April 2001. (B) Fluxes of O_2, TCO_2, NH_4^+ and dissolved inorganic nitrogen, $\Sigma(NH_4^+, NO_3^-, NO_2^-)$, measured in benthic chambers and calculated from pore water gradients in Buzzards Bay.

Figure 4. Pore water profiles have been combined at each time point to generate "composite" profiles of Mo, U, Re, Fe^{2+}, Mn^{2+} and O_2 (based on *in situ* microelectrode profiles). The dotted vertical line denotes the overlying water concentrations. Best–fit model profiles for Mo, U and Re are included for comparison. The solid line model fits used the average representative α profile, and the dashed line model fits used the contemporaneous Br–derived α profiles. In April 2001 and August 2004 the U profiles are more consistent with the average α profile than with the contemporaneous Br–derived α profile. The mechanism for removal of the added U is diffusion upward to the removal layer, followed by loss to the solid phase. This process is slow relative to the length of a chamber deployment (~4 days), and is therefore better described using a longer–term, average α instead of the contemporaneous Br–derived α profile. Because there is no Br^- data for August 2003, only the average representative α profile was used. Irrigation was not included for March 2003 since Rn–disequilibrium experiments showed no irrigation at this time of year. However, irrigation may have been significant since Br^- concentrations

in flux chambers decreased more than would be expected from only diffusion across the sediment–water interface. The absence of subcores collected from the flux chamber core at the conclusion of the deployment prevents us from constructing pore water Br^- profiles or calculating Br–derived α profiles for March 2003.

Figure 5. Solid phase profiles of metal/aluminum ratios versus depth in sediments for Fe, Mn, U, Mo and Re in Buzzards Bay. The vertical dashed lines represent the metal/Al ratios in granitic rocks (Turekian and Wedepohl, 1961), which seem to be an appropriate estimate for the incoming detrital material based on regional surveys (Moore, 1963).

Figure 6. Solid phase profiles of excess (A) ^{234}Th and (B) ^{210}Pb for March 2003, August 2003 and August 2004 in Buzzards Bay. The average excess ^{210}Pb profile is presented in plot (C), where the horizontal lines denote the standard deviation for the averages.

Figure 7. (A) Pore water profiles for excess bromide in subcores collected from below the flux chambers at the end of the deployments. Horizontal lines represent the variability among replicate subcores. The solid lines are the best–fit lines for the profiles. (B) Overall "representative" α vs. depth profile, normalized to the diffusion coefficient for Br^-. Symbols are the calculated average α values, the line is an exponential fit to these values, and the speckled region shows the difference between the "Br–normalized" Rn–based results and the Br–based values. In general, the α values based on Rn data are greater than the Br–derived values, implying deeper irrigation. This could be due to: (1) artifacts in the Rn measurements (Martin and Sayles, 2004); (2) artifacts due to the presence of the flux chamber for Br^-; (3) the short duration of the Br^- measurements (~4 days relative to ~2 weeks for Rn); or (4) variable irrigation at the Buzzards Bay site during the two decades encompassing these experiments.

Figure 8. A cartoon depicting sedimentary RSM fluxes in Buzzards Bay, including solid phase bioturbation (on the left) and exchange of dissolved species via irrigated burrows (on the right). Exchange between the solid and aqueous phases is denoted by horizontal arrows in the middle of the figure. Note that F_{prod} is the net flux of RSM to the dissolved phase from the release of RSM from the solid phase above x_p. There

1211 was no evidence in Buzzards Bay for net removal of RSM to the solid phase in
1212 sediments shallower than x_p.

1213 **Figure 9.** Seasonal differences in (A) total authigenic phase formation rate (F_{auth}), and
1214 (B) the fraction of this flux that can be attributed to direct transport from bottom
1215 waters (f_{bw}).

1216 **Figure 10.** Benthic chamber fluxes at the Buzzards Bay site compared to fluxes
1217 calculated from pore water profiles of U, Re and Mo. If small–scale spatial and
1218 temporal variability is limited, then the benthic chamber fluxes should be equivalent
1219 to the sum of the diffusive and irrigation–driven fluxes across the sediment–water
1220 interface. Irrigation was assumed to be zero in March 2003 as discussed in the Figure
1221 4 caption. The contemporaneous Br–derived α profiles were used for April 2001 and
1222 August 2004 to calculate the irrigation component of the flux across the sediment–
1223 water interface; the average representative α profile was used for August 2003. In
1224 August 2004 both the contemporaneous Br–derived and the average representative α
1225 profiles were used for comparison, with the average α profile yielding higher
1226 irrigation fluxes. The calculated Re flux for March is from pore waters separated from
1227 sediments by sectioning and centrifugation. In April, pore water Re was determined
1228 both by sectioning/centrifugation and by equilibration with a gel probe; the flux
1229 shown was calculated from the gel probe data. Near–interface Re values obtained in
1230 April from the gel probe were approximately a factor of two lower than those
1231 determined from a section–centrifuge profile; therefore, the March pore water flux
1232 obtained from a sectioned/centrifuged core may be artificially large.

1233 **Figure 11.** Pore water profiles from the sites in (A) Hingham Bay and (B) Buzzards Bay.
1234 The profiles are the average of two or three profiles for each time period and the
1235 horizontal lines represent the standard deviations. For the bottom plot in (A), the
1236 symbols are the pore water Fe concentrations whereas the line reflects the average
1237 H_2S concentration. Plot (C) shows a comparison of pore water sulfate profiles from
1238 the two sites. The vertical line is the bottom water sulfate concentration.

Figure 12. Solid phase profiles of Re (pmol/g) from (A) Buzzards and (B) Hingham bays. The profile from Buzzards Bay is the composite profile, whereas the profile from Hingham Bay is from a single sediment core collected in January 2002.

Table 1. Comparison of sampling sites in Buzzards Bay (this work) and Hingham Bay (Morford et al., 2007).

	Buzzards Bay	**Hingham Bay**
Water depth (m)	15	5
Sediment type	Silty clay[a]	Silty clay[b]
Annual temperature (^{o}C)	2–25[c]	0–16[d]
Bottom water O_2 concentrations (μM)	230–300[c]	240–380[d,e]
O_2 penetration depth (mm)	2.5–8.5[c]	~2–6[e]
Sedimentation rate (cm y^{-1})	0.05–0.3[f]	0.45 ± 0.09[g]
Solid phase organic carbon content (%)	2[h]	3.5[j]
Annually averaged organic matter oxidation rate (μmol C cm^{-2} y^{-1})[k]	390[c]	880[e]

[a]Moore, 1963; [b]Bothner et al., 1998; [c]this work; [d]Libby et al., 2002; 2003; 2004a,b; [e]Morford et al., 2007; [f]the sedimentation rate for BB was determined from the range in rates calculated from ^{14}C analyses (McNichol et al., 1988) and from ^{210}Pb analyses (Brownawell, 1986); [g]the sedimentation rate for HB was determined by the changing depth of the ^{137}Cs peak over 22 years and has been revised since Morford et al. (2007); [h]McNichol et al., 1988; [j]Kalnejais, 2005; [k]determined from TCO_2 fluxes using *in situ* benthic flux chambers; [m]determined from the average TCO_2 flux measured by a benthic chamber and calculated from the pore water profile (see Morford et al., 2007).

Table 2. RSM concentrations in overlying water (ovw) and benthic chamber samples (t=1 hr) from Buzzards Bay. When not otherwise stated, the concentration represents the analysis of one sample (n=1). In addition to the average concentration and standard deviation, the percent relative deviation [%RSD=(average/standard deviation)x100] and number of measurements (n) are included. The ranges in oceanic RSM concentrations were adjusted from average oceanic salinity (s=35) to average Buzzards Bay salinity (s=31.6). The expected Re concentration in the CASS–4 sample is derived from the literature (adjusting for the salinity of the CASS–4 sample, s=30.7).

Time	**Sample**	**[Re] (pmol kg^{-1})**	**[U] (nmol kg^{-1})**	**[Mo] (nmol kg^{-1})**
March 2003	ovw benthic chamber	37.7 36.1	12.7 ± 0.9 (n=10) 12.8	99 ± 4 (n=10) 96.3
April 2001	ovw (n=2) benthic chamber	28 ± 2 36.0	12.27± 0.09 12.2	103 ± 1 98.7
Aug 2003	ovw benthic chamber	37.6 35.3	13 ± 2 (n=9) 12.4	100 ± 5 (n=9) 103
Aug 2004	ovw benthic chamber (3A)	35.8 35.3 ± 0.1 (n=3)	11.7 12.5	98.6 100
	Ave ± std dev **%RSD** **n**	**36 ± 2** **4%** **12**	**13 ± 1** **9%** **27**	**100 ± 4** **4%** **27**
	Expected RSM conc.	35–41[a]	12.6[b]	94.5[c]
CASS-4	**Ave measured ± std dev** **%RSD** **n**	**34.6 ± 0.8**[d] **2%** **15**	**12 ± 1** **8%** **39**	**96 ± 5** **5%** **39**
	Known conc.	34–40[a]	12[e]	90 ± 9

[a]Colodner (1991), Anbar et al. (1992).
[b]Ku et al. (1977).
[c]Collier (1985)
[d]Previous measurements of Re in CASS–4 also resulted in a similar concentration (35 ± 5 pmol/kg; Morford et al., 2005).
[e]Information value only.

Table 3. Average, standard deviation and RSD of metal concentrations from replicate dissolution and analysis of the standard sediment PACS–2 (n=6) are compared with the known concentrations. The Al, Fe and Mn analyses were completed using ICP–OES, and the U, Mo and Re concentrations were determined using ICP–MS.

	[Al]	**[Fe]**	**[Mn]**	**[U]**	**[Mo]**	**[Re]**
	(μmol/g_{sed})			**(nmol/g_{sed})**		**(pmol/g_{sed})**
Ave measured ± std dev (%RSD)	2,420 ± 30 (1%)	720 ± 10 (2%)	7.81 ± 0.09 (1%)	9.3 ± 0.3 (3%)	54 ± 3 (5%)	27.5 ± 0.5 (2%)
Known conc.	2,400 ± 100	730 ± 10	8.0 ± 0.4	13*	57 ± 3	na

*Information value only; na = not available

Table 4. Bottom water temperatures and best–fit porosity parameters used for the RSM pore water model profiles.

Time	**Temp (°C)**	**Porosity parameters[a]**			**ν–1[b]**
		a	**b**	**c**	
March 2003	8	0.732	0.121	0.111	2.48
April 2001	14	0.736	0.183	0.356	1.38
August 2003	18	0.736	0.160	0.247	1.74
August 2004	20	0.779	0.163	0.649	1.60

[a]The porosity (ϕ) at any depth (x) can be solved as $\phi = a + be^{-cx}$ where the parameters (a, b and c) are determined by least–squares fits to the measured porosity versus depth profiles (Martin and Sayles, 1987; Martin and Banta, 1992). [b]The effect of sediment tortuosity on the diffusion coefficient for seawater (D_{sw}), which is assumed to be equal to the diffusion coefficient in pore water, is experimentally determined by resistivity measurements. The ratio of sediment resistivity to that of pore water is equivalent to the formation factor (F) (McDuff and Ellis, 1979) and is used to calculate the diffusion coefficient in sediments: $D_{sed} = \frac{D_{sw}}{\phi F} = D_{sw}\phi^{\nu-1}$. The latter half of the equation is derived from the Winsauer relationship $F = c\phi^{-\nu}$.

Table 5. Irrigation rate parameters determined for Buzzards Bay (this work; Martin and Sayles, 1987).

Experiment	**α_1 (y^{-1})**	**α_2 (cm^{-1})**	**L_{max} (cm)**	**Comments**
Oct 1982[a]	110	0.380	NA	
June 1983[a]	151	0.190	NA	
Sept 1983[a]	56.7	0.230	NA	
June 1984[a]	11.6	0	NA	
Sept. 1996 #2[b]	135	0.497	15	
Oct 1996 #4[b]	77.0	0.182	15	Apparent leak from chamber
April 2001 #3[b]	3.72	-0.162	11.50	Possible transient event
Aug 2004 #3[b]	50.1	0	3.0	
Aug 2004 #4[b]	91.0	0	3.0	

NA. Not applicable. In describing the data, no maximum irrigation depth was invoked and only α_1 and α_2 were used as fitting parameters.

a. Irrigation rate parameters determined for Buzzards Bay using ^{222}Rn / ^{226}Ra disequilibrium measurements (Martin and Sayles, 1987).

b. Irrigation rate parameters determined for Buzzards Bay using benthic chamber bromide experiments (this work).

Table 6. Solid phase RSM concentrations for the Buzzards Bay site. Depth (cm) is measured below the sediment–water interface. Al, Fe and Mn concentrations are in μmol/g, U and Mo concentrations are in nmol/g and Re concentrations are in pmol/g. Detrital concentrations (average granite, Turekian and Wedepohl, 1961; except for Re, Koide et al., 1986) are included for comparison. Note: '–' denotes not measured.

Date	Depth	[Al]	[Fe]	[Mn]	[U]	[Mo]	[Re]
March 2003	0.82	2353	580	7.12	11.3	8.43	19.0
	0.82	2376	584	7.04	–	–	–
	2.20	2400	573	6.76	12.2	11.6	18.9
	2.20	2405	573	6.73	11.8	12.1	19.0
	4.33	2424	555	6.70	11.9	16.2	20.6
	6.65	2393	535	6.83	13.2	16.4	23.6
	6.65	2361	555	6.63	12.2	15.4	22.0
	10.75	2373	569	6.58	13.5	17.4	27.3
	10.75	2390	578	6.92	–	–	–
	12.12	2416	580	6.97	12.9	15.6	27.6
	15.13	2392	569	6.74	14.3	14.6	27.1
	18.43	2308	534	6.63	13.6	14.1	24.8
	22.30	2364	566	6.88	15.6	27.4	34.4
April 2001	**Depth**	**[Al]**	**[Fe]**	**[Mn]**	**[U]**	**[Mo]**	**[Re]**
	0.96	2283	586	7.90	10.8	9.92	16.9
	0.96	2283	589	7.90	10.8	9.80	16.5
	1.88	2409	552	6.94	11.0	9.04	19.0
	4.28	2357	535	6.79	12.2	13.3	20.9
	4.28	–	–	–	12.1	13.2	21.2
	6.02	2405	541	6.79	11.9	15.2	22.1
	8.02	2298	509	6.37	11.7	17.8	22.4
	10.02	2346	521	6.66	12.0	14.7	23.1
	13.52	2350	543	6.73	13.0	17.9	26.8
	13.52	2327	535	6.59	12.7	17.9	27.1
	17.52	2357	505	6.59	13.6	19.7	32.1
	19.52	2257	517	6.57	13.3	17.1	28.8
	21.52	2201	507	6.43	13.1	20.4	29.5
August 2003	**Depth**	**[Al]**	**[Fe]**	**[Mn]**	**[U]**	**[Mo]**	**[Re]**
	0.96	2294	564	7.45	10.9	8.97	16.0
	0.96	2339	586	7.54	–	–	–
	2.11	2378	568	6.92	11.8	8.69	17.9
	4.52	2408	564	6.81	12.2	12.9	19.7
	5.78	2397	559	6.84	12.7	14.2	20.6
	7.05	2350	534	6.50	12.6	16.5	22.5
	8.32	2216	480	6.27	12.5	20.3	22.6
	8.32	2242	525	6.08	11.8	18.6	20.8
	10.44	2249	530	6.63	12.3	22.0	22.2
	12.61	2344	541	6.55	13.2	19.6	25.1
	14.28	2389	559	6.87	13.7	21.0	27.0
	16.53	2336	557	6.86	13.7	23.6	28.7
	16.53	2424	589	6.61	13.8	24.2	29.9
	16.53	2361	569	6.70	–	–	–
	18.78	2376	541	6.70	14.2	20.3	33.0

August 2004	Depth	[Al]	[Fe]	[Mn]	[U]	[Mo]	[Re]
	0.93	2272	553	6.95	10.3	8.30	15.1
	2.32	2279	494	6.32	11.0	9.10	16.3
	4.26	2313	517	6.37	12.0	13.2	19.6
	6.10	2346	539	6.66	13.1	19.3	22.4
	8.23	2598	616	7.44	14.5	25.6	27.5
	10.37	2316	568	6.46	13.3	19.4	22.7
	13.90	2324	562	6.83	13.2	25.7	25.7
	17.90	2339	557	6.94	14.0	18.7	29.6
	21.90	2339	580	7.06	14.7	34.2	37.1
Average Granite		***3000***	***530***	***10***	***13***	***10***	***0.5***

Table 7. Solid phase authigenic RSM concentrations, solid phase accumulation rates, and modeled authigenic formation rates for Buzzards Bay are compared to the authigenic concentrations and accumulation rates for Hingham Bay (Morford et al, 2007).

	Buzzards Bay			**Hingham Bay**	
	Authigenic concentration[a] ($nmol/g_{sed}$)	**Authigenic accumulation rate**[b] ($nmol/cm^2/y$)	**Modeled authigenic formation rate**[c] ($nmol/cm^2/y$)	**Authigenic concentration**[d] ($nmol/g_{sed}$)	**Authigenic accumulation rate**[b] ($nmol/cm^2/y$)
U	4.2 ± 0.1	0.4 ± 0.1	1.9 ± 0.8	5 ± 2	1.3 ± 0.05
Mo	11 ± 3	1.1 ± 0.5	4 ± 1	28 ± 6	8 ± 2
Re ($x10^{-3}$)	29 ± 3	3 ± 1	4 ± 3	20 ± 2	5.6 ± 0.5

[a]RSM and aluminum concentrations are used in concert with metal/Al detrital ratios to calculate the authigenic RSM concentrations as: $[RSM]_{auth} = [RSM]_{measured} - \left\{ \left(\frac{[RSM]}{[Al]} \right)_{detrital} * [Al]_{measured} \right\}$. The measured concentrations are the average values below 15 cm. The detrital concentrations are from average granite (Turekian and Wedepohl, 1961), based on the predominate rock type bordering Buzzards Bay (Moore, 1963), except for the detrital Re concentration which is assumed to be $5x10^{-13}$ mol g^{-1} (Koide et al., 1986).

[b]The solid phase accumulation rates are calculated as: $F_{auth} = [RSM]_{auth} s(1-\phi)\rho$. The sedimentation rate for Buzzards Bay (s) is assumed to be 0.2 cm/y, which is intermediate between the literature sedimentation rates (0.05 cm/y, McNichol et al., 1988; 0.3 cm/y, Brownawell, 1986). The solid phase density (ρ) is 2.6 g/cm^3, and the porosity (ϕ) is 0.75 $cm^3_{water}/cm^3_{sediment}$. The sedimentation rate for Hingham Bay is from Table 1, and ϕ is 0.77 $cm^3_{water}/cm^3_{sediment}$.

[c]The modeled authigenic formation rate is calculated as the formation rate attributable to direct transport from bottom waters, or $f_{bw}*F_{auth}$ (Table 11).

[d]The authigenic U and Mo concentrations for Hingham Bay are from Morford et al. (2007). The Hingham Bay authigenic U and Mo concentrations may be conservative, since they were calculated as the difference between the average surface and deep concentrations and do not include possible authigenic enrichment in surface sediments (Morford et al., 2007). The Re solid phase authigenic concentration and accumulation rate are presented in this manuscript and are calculated in the same manner as described for Buzzards Bay.

Table 8. The best–fit model values for the five variable parameters used for fitting the RSM composite profiles: reaction parameters k_r (U, Mo: nmol cm_{pw}^{-3} y^{-1}; Re: pmol cm_{pw}^{-3} y^{-1}) and k_p (y^{-1}), the minimum pore water concentration in the profile (C_{min}, U, Mo: nmol kg^{-1}; Re: pmol kg^{-1}), and the boundaries of the layer in which RSM are removed from pore waters to the solid phase [upper limit = x_p (cm); lower limit = x_s (cm)]. The resultant diffusive fluxes across the sediment–water interface (F_0) and at the depth of removal (F_{xp}) are also presented (pmol cm^{-2} y^{-1}). When there is no additional source of RSM to pore waters via release from solid phases in surface sediments (k_r=0), then the flux across the sediment–water interface must be equivalent to the diffusive flux calculated at the depth of removal (F_0=F_{xp}).

Fit Results			**k_r**	**k_p**	**C_{min}**	**x_p**	**x_s**	**F_o**	**F_{xp}**
March 2003	Re		4.96 x 10^5	94.8	4.39	0.17	3.80[c]	+65700	-6930
	Mo		0	543	89.3	0	7.50	-2320	-2320
	U		25.3	306	1.6	1.03	3.22	-691	-713
April 2001[a]	Re	αBr	25000	92.1	7.14	0.95	11.9	+15600	-5820
		αav	1.94 x 10^5	80.3	7.14	0.34	16.9	+52300	-7470
	Mo	αBr	466	1380	37.8	2.32	6.75	-3130	-4180
		αav	7.81	1450	37.8	2.26	6.79	-3110	-4590
	U	αBr	0	206	2.55	0	8.77	-1810	-1810
		αav	0	292	2.55	0	9.03	-2090	-2090
Aug 2003	Re		0	56.8	7.12	0	17.9	-2510	-2510
	Mo		7780	512	30.2	1.67	6.66	+2440	-9160
	U[b]	D_{hi}	0.469	3390	1.37	1.39	6.20	-1120	-1340
		D_{lo}	0.375	1490	1.37	1.37	6.23	-491	-583
Aug 2004[a]	Re	αBr	158	158	3.99	0.16	6.31	-5410	-5440
		αav	1010	182	3.99	0.11	23.4	-5670	-5780
	Mo	αBr	5700	550	10.6	1.46	3.86	-2380	-10500
		αav	5300	604	10.6	1.50	7.10	-2530	-10500
	U	αBr	1.56	1490	0.83	1.00	2.86	-1610	-1730
		αav	0.156	1040	0.83	0.90	6.86	-1620	-1750

a The April 2001 and August 2004 model fits were calculated using the contemporaneous Br–derived and the average representative α profiles.

b The August 2003 U model was fitted to the pore water composite profile using both the higher diffusion coefficient based on MoO_4^{2-} and the lower diffusion coefficient from UO_2^{2+} (Li and Gregory, 1974). **c** The thin Re removal zone is a limitation of the model due to the model's inability to allow for slower removal of Re in conjunction with the size and sharpness of the surface pore water Re peak. The resulting model fit is poor and the bottom of the removal layer (x_s) is too shallow relative to the apparent curvature of the Re profile.

Table 9. The depths of onset of removal (x_p) are calculated from the model fits to the composite pore water profiles.

Time	**Depth of onset of removal (cm)**		
	Mo	**U**	**Re**
March 2003	NR	1.03	0.17
April 2001	2.30	0	0.65
August 2003	1.67	1.39	0
August 2004	1.48	0.95	0.14
Average	**1.8 ± 0.4**	**0.8 ± 0.6**	**0.2 ± 0.3**

NR: The pore water profile of Mo in March 2003 suggests only limited removal from pore waters during this time point, so the depth of onset of removal is not included.

Table 10. The extent of removal is derived from the model output for the minimum pore water concentration (C_{min}) and the bottom water concentration (C_0). The averages and standard deviations for the extent of removal at Buzzards Bay are compared with the averages determined at the Hingham Bay site (Morford et al., 2007).

Time	**Extent of removal (C_{min}/C_0)**		
	Mo	**U**	**Re**
March 2003	0.90	0.13	0.12
April 2001	0.38	0.20	0.20
August 2003	0.30	0.11	0.20
August 2004	0.11	0.07	0.11
Buzzards Bay			
Average ± standard deviation	**0.4 ± 0.3**	**0.13 ± 0.05**	**0.16 ± 0.05**
Hingham Bay			
Average ± standard deviation	**0.10 ± 0.03**	**0.23 ± 0.04**	**0.34 ± 0.05**

Table 11. RSM fluxes are derived from model fits to composite pore water profiles (Mo, U: nmol/cm^2/y; Re: pmol/cm^2/y) as described in the text, and contributions to removal are calculated as the flux divided by the authigenic RSM formation rate (F_{auth}).

	FLUXES						CONTRIBUTIONS TO REMOVAL				
Time	**F_0**	**F_{prod}**	**F_{xp}**	**F_{irr}**	**F_{xs}**	**F_{auth}**	**f_{prod}**	**f_{xp}**	**f_{irr}**	**f_{xs}**	**f_{bw}**
Mo											
March 03	2.31	0.00	2.31	0.00	0.00	2.31	0.00	1.00	0.00	0.00	1.00
April 01	3.13	0.92	4.18	0.81	1.30	6.29	0.15	0.66	0.13	0.21	0.65
Aug 03	-2.44	11.05	9.16	4.28	1.49	14.93	0.58	0.61	0.29	0.10	0.32
Aug 04	2.39	7.07	10.53	0.41	9.53	20.47	0.35	0.51	0.02	0.47	0.19
U											
March 03	0.69	0.020	0.71	0.00	0.02	0.73	0.03	0.97	0.00	0.03	0.95
April 01	1.84	0.000	1.84	0.25	0.06	2.15	0.00	0.86	0.12	0.03	0.97
Aug 03	1.12	0.001	1.34	0.85	0.06	2.25	0.00	0.60	0.38	0.03	0.97
Aug 04	1.61	0.001	1.73	0.75	0.24	2.72	0.00	0.64	0.28	0.09	0.91
Re											
March 03	-65.70	72.50	6.93	0.00	0.00	6.93	0.98	1.00	0.00	0.00	0.00
April 01	-15.61	20.20	5.82	1.57	0.00	7.39	0.62	0.79	0.21	0.00	0.38
Aug 03	2.51	0.00	2.51	3.38	0.00	5.89	0.00	0.43	0.57	0.00	1.00
Aug 04	5.41	0.02	5.44	2.42	0.00	7.86	0.00	0.69	0.31	0.00	1.00

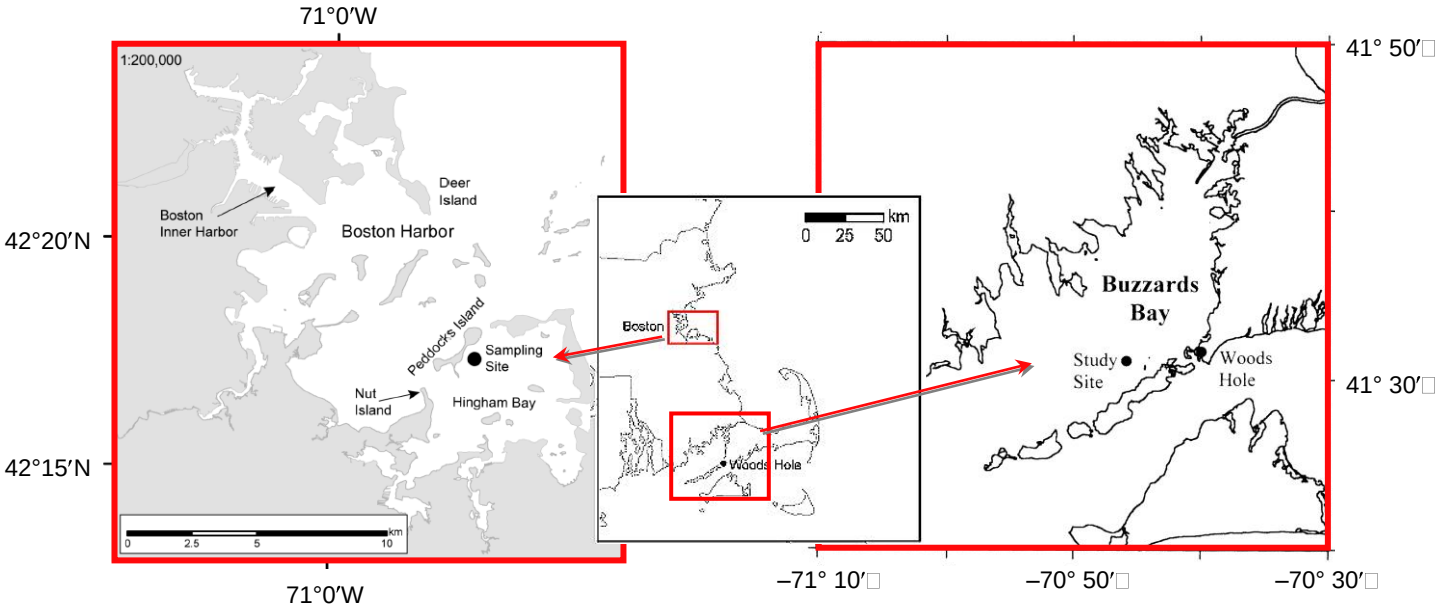
71°0′W
1:200,000
Deer
Island
Boston
Inner Harbor
Boston Harbor
42°20′N
Peddock's Island
Sampling
Site
Nut
Island
Hingham Bay
42°15′N
0 2.5 5 10 km
71°0′W
km
0 25 50
Boston
Woods Hole
Buzzards
Bay
Study
Site
Woods
Hole
41° 50′
41° 30′
–71° 10′
–70° 50′
–70° 30′

Figure 1.

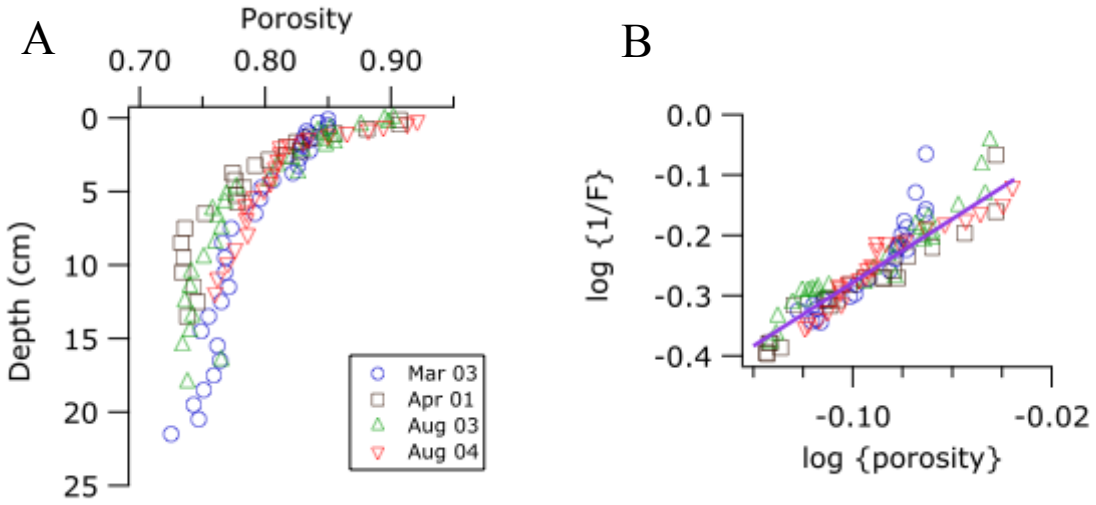
A
Porosity
0.70
0.80
0.90
0
5
10
15
20
25
Depth (cm)
Mar 03
Apr 01
Aug 03
Aug 04
B
0.0
-0.1
-0.2
-0.3
-0.4
log {1/F}
-0.10
-0.02
log {porosity}

Figure 2.

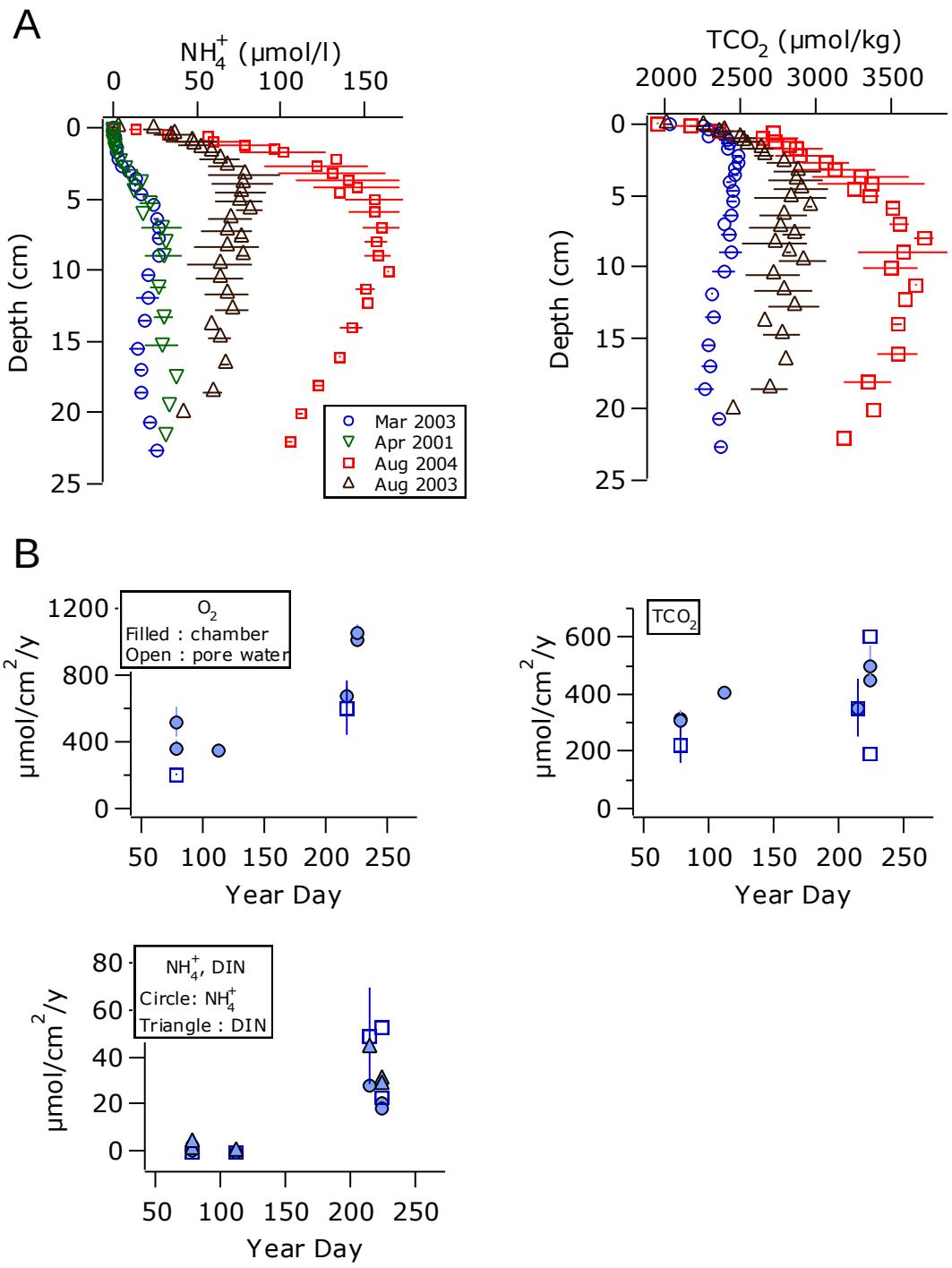
A
NH_4^+ (µmol/l)
0
50
100
150
Depth (cm)
0
5
10
15
20
25
Mar 2003
Apr 2001
Aug 2004
Aug 2003
TCO_2 (µmol/kg)
2000
2500
3000
3500
B
O_2
Filled : chamber
Open : pore water
µmol/cm^2/y
1200
800
400
0
50
100
150
200
250
Year Day
TCO_2
600
400
200
NH_4^+, DIN
Circle: NH_4^+
Triangle : DIN
80
60
40
20

Figure 3.

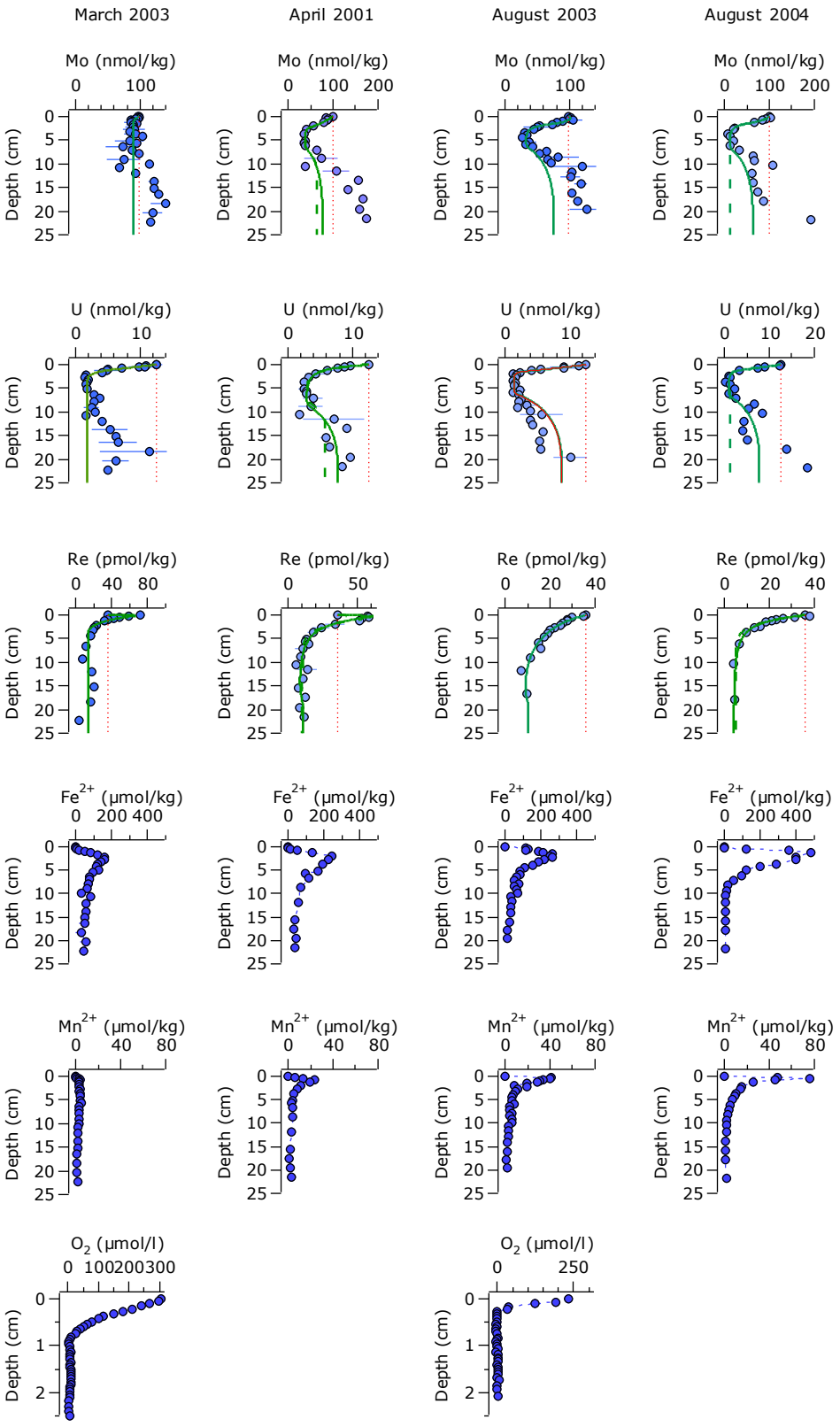
March 2003
April 2001
August 2003
August 2004
Mo (nmol/kg)
U (nmol/kg)
Re (pmol/kg)
Fe2+ (µmol/kg)
Mn2+ (µmol/kg)
O2 (µmol/l)
Depth (cm)

Figure 4.

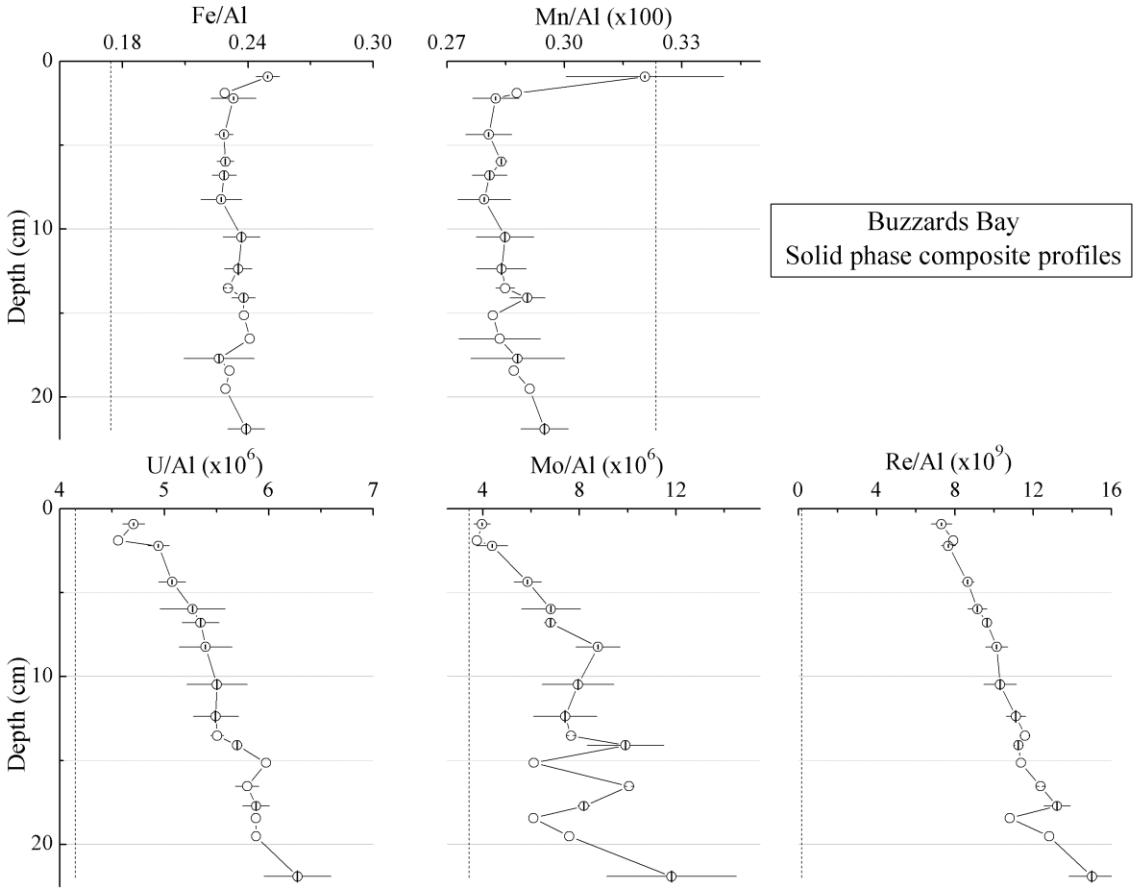
Fe/Al
0.18
0.24
0.30
Mn/Al (x100)
0.27
0.30
0.33
Depth (cm)
0
10
20
Buzzards Bay
Solid phase composite profiles
U/Al (x10^6)
4
5
6
7
Mo/Al (x10^6)
4
8
12
Re/Al (x10^9)
0
4
8
12
16

Figure 5.

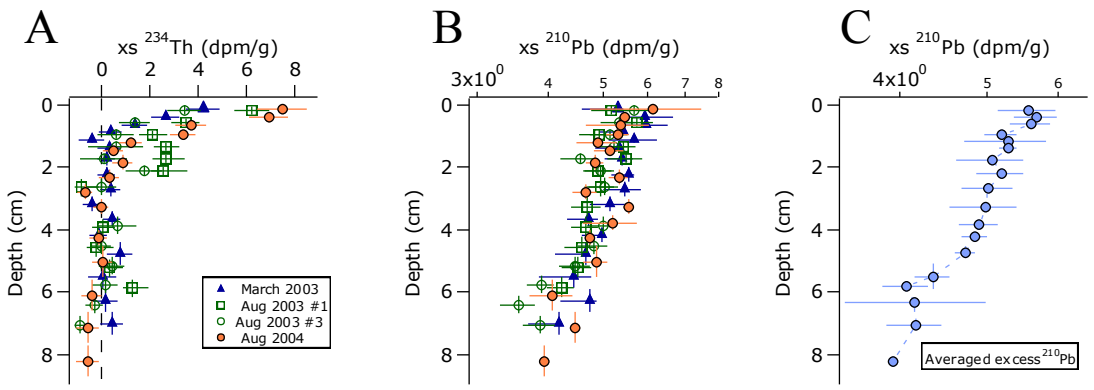
A
xs 234Th (dpm/g)
0 2 4 6 8
Depth (cm)
0 2 4 6 8
March 2003
Aug 2003 #1
Aug 2003 #3
Aug 2004
B
xs 210Pb (dpm/g)
3x10^0
4 5 6 7 8
Depth (cm)
0 2 4 6 8
C
xs 210Pb (dpm/g)
4x10^0
5 6
Depth (cm)
0 2 4 6 8
Averaged excess 210Pb

Figure 6.

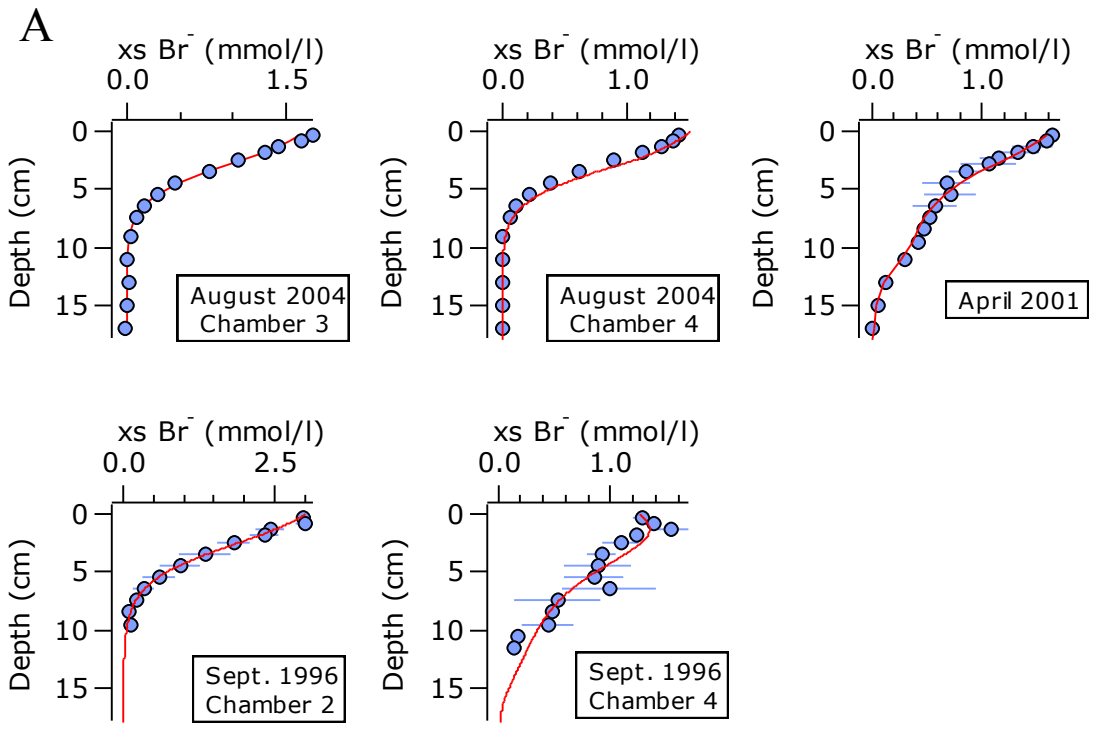
A
xs Br- (mmol/l)
0.0
1.5
Depth (cm)
0
5
10
15
August 2004
Chamber 3
xs Br- (mmol/l)
0.0
1.0
August 2004
Chamber 4
xs Br- (mmol/l)
0.0
1.0
April 2001
xs Br- (mmol/l)
0.0
2.5
Sept. 1996
Chamber 2
xs Br- (mmol/l)
0.0
1.0
Sept. 1996
Chamber 4

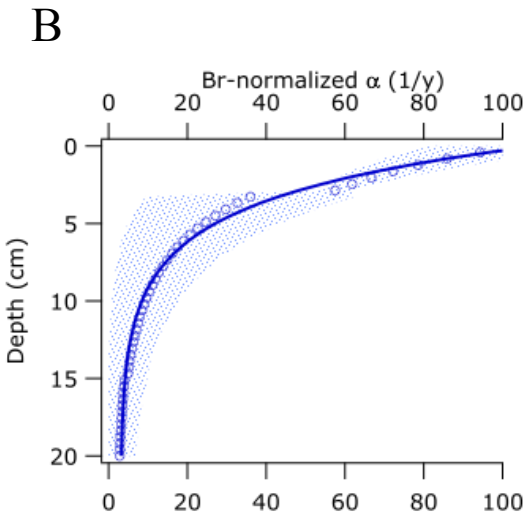
B
Br-normalized α (1/y)
0
20
40
60
80
100
Depth (cm)
0
5
10
15
20

Figure 7.

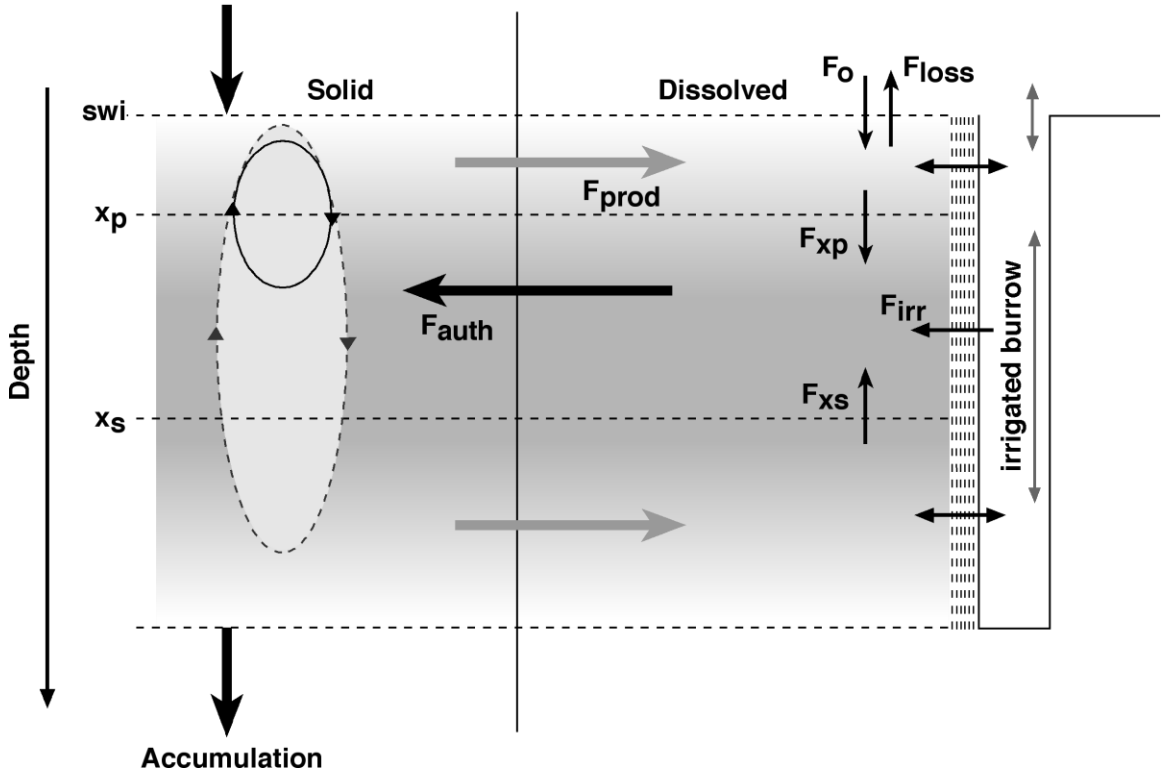
Solid
Dissolved
swi
x_p
x_s
Depth
F_{prod}
F_{auth}
F_o
F_{loss}
F_{xp}
F_{irr}
F_{xs}
irrigated burrow
Accumulation

Figure 8.

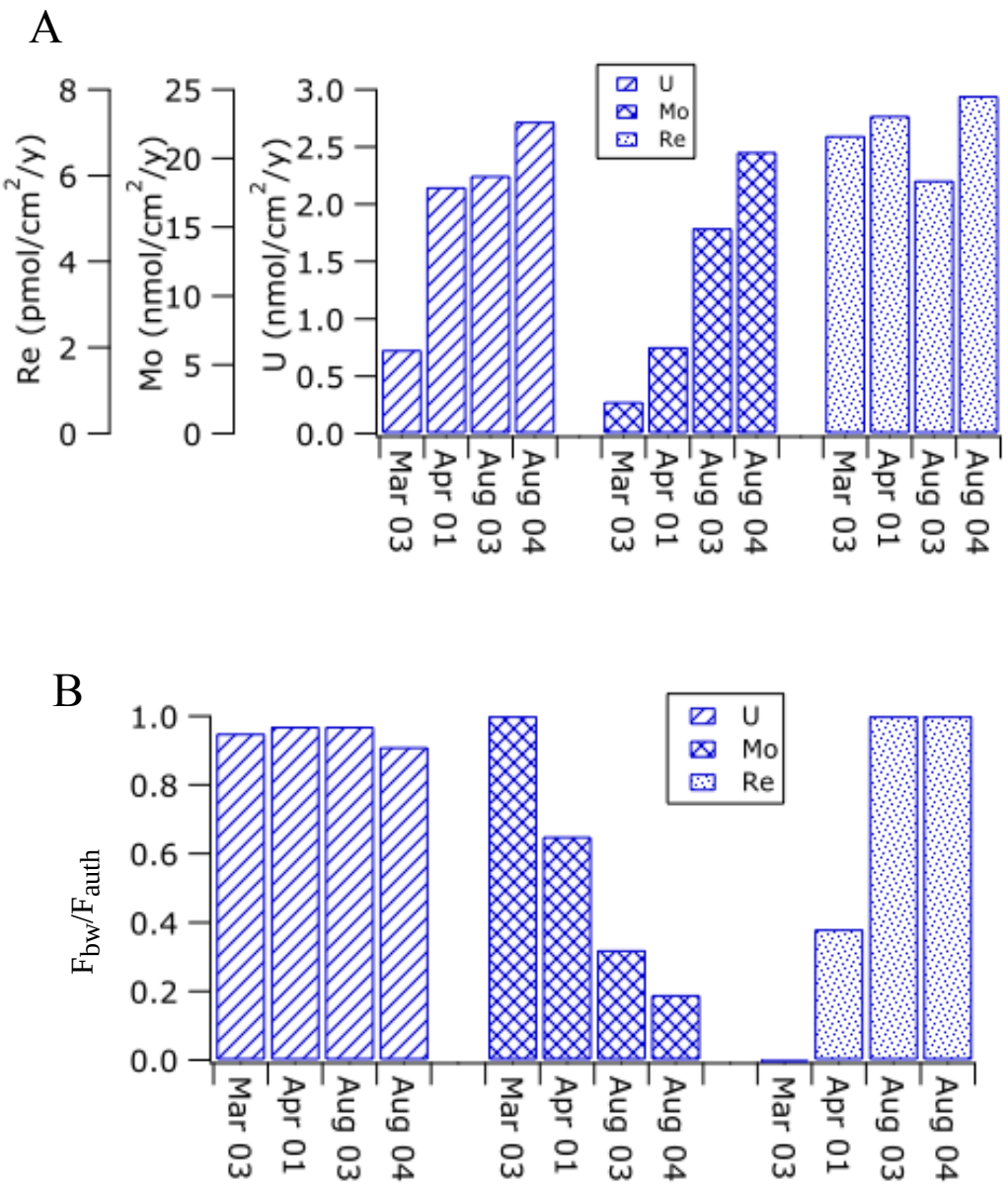
A
Re (pmol/cm2/y)
Mo (nmol/cm2/y)
U (nmol/cm2/y)
U
Mo
Re
Mar 03
Apr 01
Aug 03
Aug 04
B
Fbw/Fauth
U
Mo
Re
Mar 03
Apr 01
Aug 03
Aug 04

Figure 9.

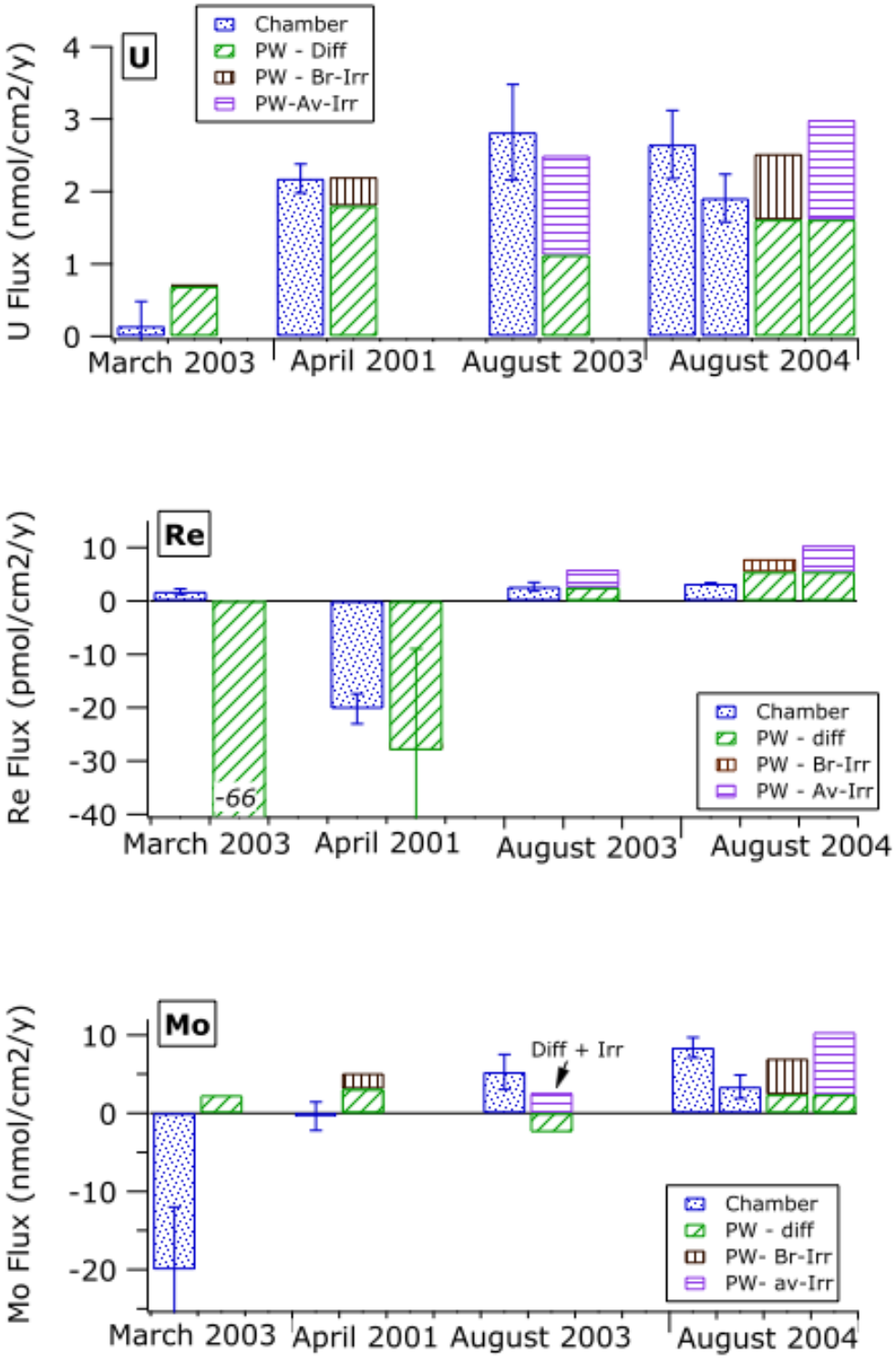
U
Chamber
PW - Diff
PW - Br-Irr
PW-Av-Irr
U Flux (nmol/cm2/y)
4
3
2
1
0
March 2003
April 2001
August 2003
August 2004
Re
Re Flux (pmol/cm2/y)
10
0
-10
-20
-30
-40
-66
Chamber
PW - diff
PW - Br-Irr
PW - Av-Irr
March 2003
April 2001
August 2003
August 2004
Mo
Mo Flux (nmol/cm2/y)
10
0
-10
-20
Diff + Irr
Chamber
PW - diff
PW- Br-Irr
PW- av-Irr
March 2003
April 2001
August 2003
August 2004

Figure 10.

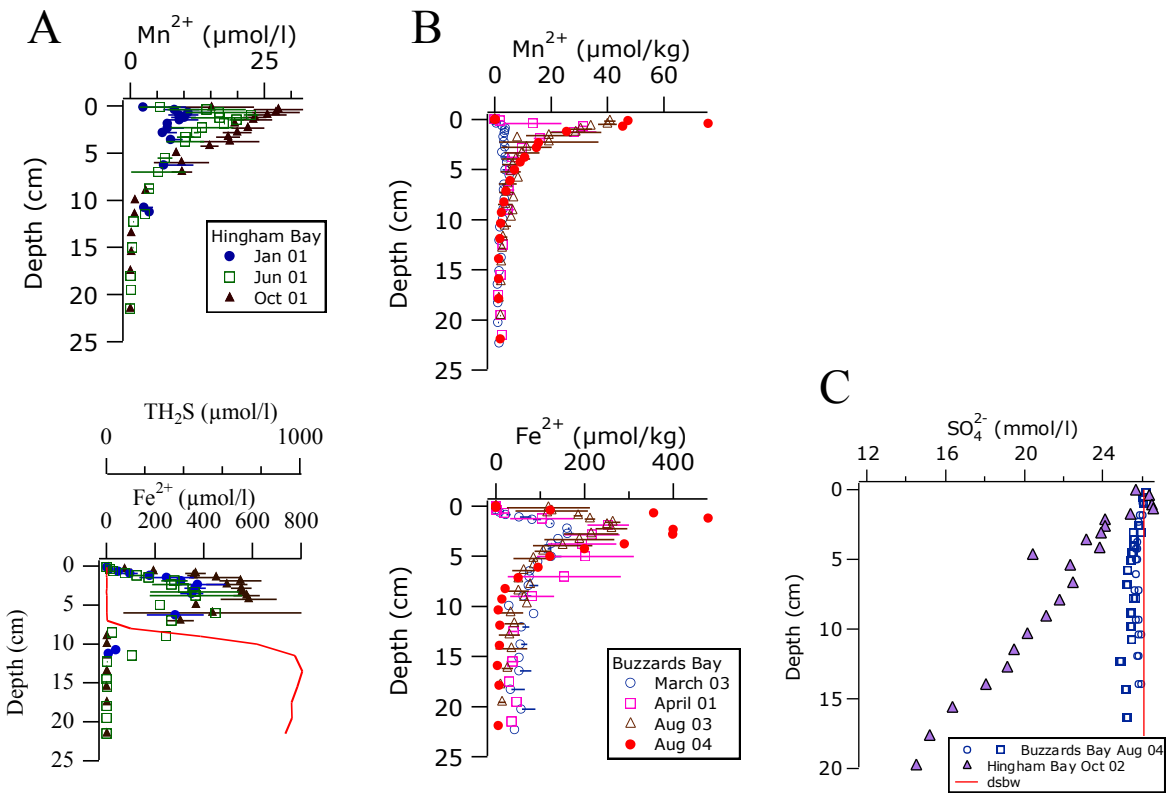
A
Mn2+ (µmol/l)
0
25
Depth (cm)
Hingham Bay
Jan 01
Jun 01
Oct 01
TH2S (µmol/l)
0
1000
Fe2+ (µmol/l)
0 200 400 600 800
B
Mn2+ (µmol/kg)
0 20 40 60
Fe2+ (µmol/kg)
0 200 400
Buzzards Bay
March 03
April 01
Aug 03
Aug 04
C
SO4 2- (mmol/l)
12 16 20 24
Buzzards Bay Aug 04
Hingham Bay Oct 02
dsbw

Figure 11.

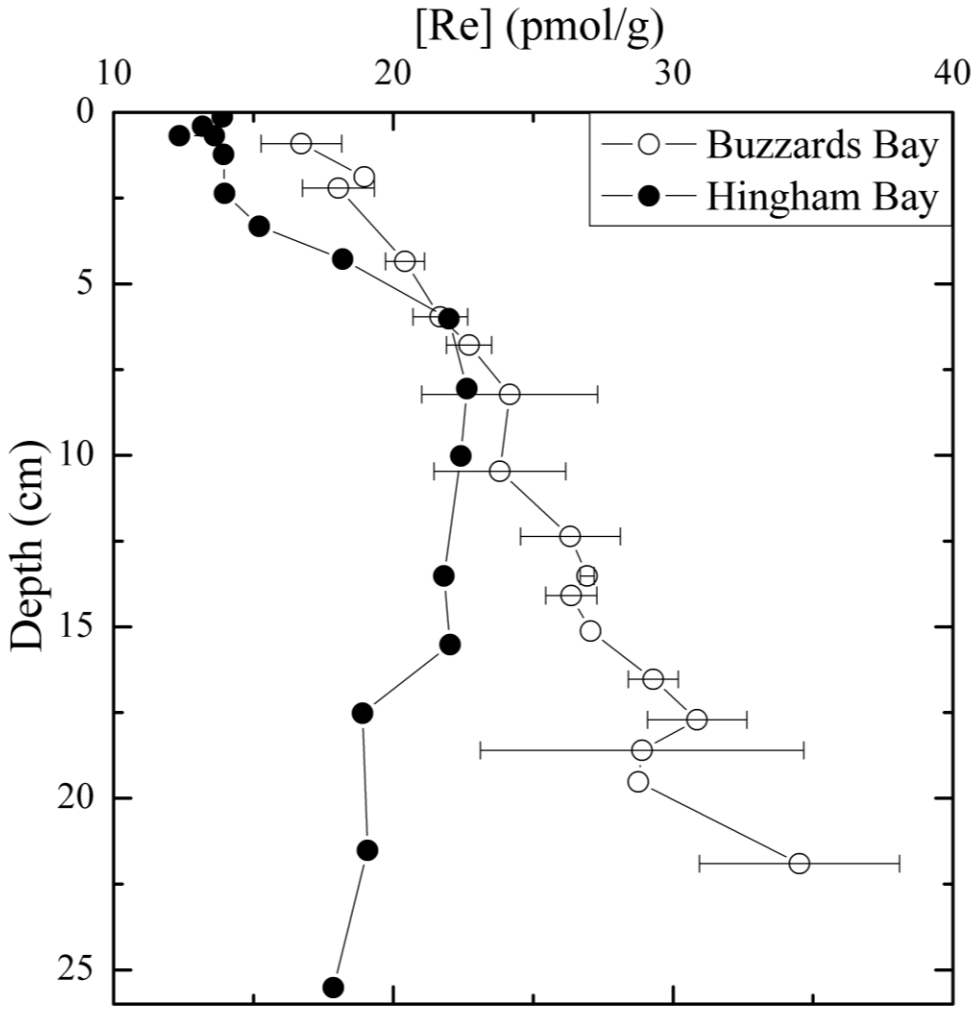
[Re] (pmol/g)
10
20
30
40
0
5
10
15
20
25
Depth (cm)
Buzzards Bay
Hingham Bay

Figure 12.